ATOMIC BEAM STUDIES OF SILVER-109m AND CESIUM-138

ATOMIC BEAM STUDIES OF SILVER-109m AND CESIUM-138

by

GLEN MONETTE STINSON, B.A.Sc., M.Sc.

A Thesis

Submitted to the Faculty of Graduate Studies

in Partial Fulfilment of the Requirements

for the Degree

Doctor of Philosophy

McMaster University

March, 1966

DOCTOR OF PHILOSOPHY (1966) (Physics)

McMaster University
Hamilton, Ontario

TITLE: Atomic Beam Studies of Silver-109m and Cesium-138

AUTHOR: Glen Monette Stinson, B.A.Sc. (University of Toronto)
M.Sc. (University of Waterloo)

SUPERVISOR: Dr. R.G. Summers-Gill

NUMBER OF PAGES: viii, 87

SCOPE AND CONTENTS:

Atomic beam magnetic resonance techniques have been used to investigate the properties of the 41-second isomeric state of silver-109 and the 32-minute ground state of the fission product cesium-138. A description of the apparatus and of the atomic beam method for the determination of nuclear moments is given.

The results obtained for silver-109m are:

$$I = 7/2 \qquad a(^2S_{1/2}) = 9477 \pm 13 \quad \text{Mc/sec}$$

$$\mu_I \text{ (uncorrected)} = 4.31 \pm 0.04 \quad \text{nuclear magnetons}$$

$$^{109}\Delta_{109m} = -(1.1 \pm 1.2)\% .$$

The value of the moment confirms that the proton configuration is $(g_{9/2})^{-3}_{7/2}$. In the course of this experiment, multiple quantum Zeeman transitions were observed between levels in both the $F = I + 1/2$ and $F = I - 1/2$ hyperfine multiplets.

The results obtained for cesium-138 are:

$$I = 3 \qquad \Delta\nu = 1650 \begin{matrix} + 650 \\ - 250 \end{matrix} \quad \text{Mc/sec}$$

$$|\mu_I| \text{ (uncorrected)} = 0.45\ ^{+0.18}_{-0.07} \quad \text{nuclear magnetons.}$$

For these experiments simultaneous detection of both the resonant and thrown out portions of the beam was used for the first time in this laboratory.

ACKNOWLEDGEMENTS

I should like to express my appreciation to all those who have made this research possible:

To Dr. R.G.Summers-Gill for suggesting this project and for his unfailing interest and helpful suggestions in all phases of this work;

To Dr. J. A. Cameron for many helpful discussions;

To Dr. N. P. Archer for supplying the cesium-138 sources;

To Mr. J. C.Waddington, Mr. A. R. Pierce, Mr.A.R. Mufti and Mr. R.G.H. Robertson for their assistance during the course of these experiments ;

To the reactor staff for providing the many radioactive sources;

To my wife, Mary, for her unfailing patience and for her encouragement when it was needed most.

I would like to acknowledge financial assistance received from the Department of Physics of McMaster University and from the Ontario Government. This research was made possible by grants to the group from the National Research Council of Canada.

TABLE OF CONTENTS

TABLE OF CONTENTS (Continued)

LIST OF TABLES

LIST OF FIGURES

CHAPTER I

INTRODUCTION

The origin of atomic beam spectroscopy can be traced to the experiments of Stern and Gerlach which showed the spatial quantization of the electronic magnetic moment (Gerlach and Stern, 1921). In 1938 Rabi introduced the atomic beam magnetic resonance technique (Rabi et al, 1938). This technique allows precise measurement of nuclear and electronic multipole moments through their effect on the hyperfine structure of electronic states. The adaption of this technique to the study of radioactive isotopes (Bellamy and Smith, 1953) has greatly increased the scope of the atomic beam field. Thus, atomic beam resonance experiments are a major source of nuclear data. The measured values of nuclear spin and multipole moments may be used as a test upon which theories of nuclear structure either stand or fall.

The study of silver-109m is an extension of the study of odd-proton nuclei below the closed proton shell at Z = 50. In this group, this work was begun by King and Cameron with the study of indium-115m, -117m, and -117 (King, 1960; Cameron, 1962) following similar studies of other indium isotopes at Columbia University, the University of California, and the Argonne National Laboratory. These silver experiments were initiated with the prospect of observing any effects on nuclear properties which might arise as one moves further away from the closed proton

shell. A comparison between indium and silver would be most useful.

The silver beam was produced by diffusing silver from irradiated natural palladium. No carrier silver was used.

The silver-109m experiments were originally to be followed by a study of silver-111m. Test runs showed, however, that the latter experiment could not be done using natural palladium as a source. At the present time, palladium enriched in palladium-110 is not available.

The cesium-138 experiments were undertaken for two reasons. First, the shell model does not make explicit prediction of the spin of odd-odd nuclei. Consequently, information concerning the neutron-proton interaction can be obtained from a study of the spins of such nuclei. Second, since cesium-138 is the daughter of the fission product xenon-138, a relatively small source was available. Cesium-138 also has a short half-life (32 minutes). Thus, the cesium-138 experiments were attempted in order to show that short-lived low abundance fission products could be investigated with atomic beam techniques.

In the course of the cesium-138 experiments, the detection technique was modified in order to allow simultaneous collection of the resonant atoms and a sample of the non-resonant beam. This was the first use of that technique in this group.

CHAPTER II

NUCLEAR MOMENTS AND NUCLEAR MODELS

A nucleus containing A nucleons consists of Z protons and (A-Z) neutrons moving about in a roughly spherical volume of radius $1.2\ A^{1/3} \times 10^{-13}$ centimeters. As a result of this motion of its constituent particles, the nucleus possesses both a charge density and a current density. The nuclear charge density is associated with the protons only and the nuclear current density with the motion of the protons and with the spins of both the protons and the neutrons. It is through these charge and current densities that the nucleus interacts with an electromagnetic field such as, for example, that of the atomic electrons.

It is more convenient, however, to express the interaction of the nucleus and field in terms of electromagnetic moments. In this manner, the interaction energy is expressed as a sum of terms proportional to the nuclear multipole moments. This method is convenient since successive terms in the summation diminish rapidly in size. In any event, the quantum mechanical series terminates after a few terms.

The general electric and magnetic multipole operators of order k are given by

$$Q_k^m = e \sum_{i=1}^{Z} r_i^k\, Y_k^m\,(\theta_i,\phi_i)$$

$$M_k^m = \mu_N \sum_{i=1}^{A} \nabla\left(r_i^k\, Y_k^m\,(\theta_i,\phi_i)\right)\cdot\left[g_\ell \frac{2\vec{\ell}_i}{k+1} + g_s \vec{s}_i\right] . \qquad (2.1)$$

In these expressions, the coordinates of the i^{th} nucleon are (r_i,θ_i,ϕ_i) and $Y_k^m\,(\theta_i,\phi_i)$ is a spherical tensor of rank k and projection m.

The orbital angular momentum of the i^{th} nucleon is designated $\vec{\ell}_i$ and the spin and orbital gyromagnetic ratios are g_s and g_ℓ respectively. The electronic charge is e and the nuclear magneton is μ_N. Because $Y_k^m(\theta_i,\phi_i)$ has parity $(-)^k$, it follows from equations (2-1) that Q_k^m and M_k^m have parity $(-)^k$ and $(-)^{k+1}$ respectively. Thus, since odd parity operators have zero expectation value in states of definite parity, it follows that even electric moments and odd magnetic moments are the only observable static multipole moments.

Although, classically, there are an infinite number of terms in the multipole expansion, quantum-mechanical considerations limit the number of terms appearing in the expansion. The expectation value of the multipole operator Q_k^m in a nuclear state $|IM>$ can be evaluated using the Wigner-Eckart theorem:

$$\langle IM | Q_k^m | IM \rangle = (-)^{I-M} \begin{pmatrix} I & k & I \\ -M & m & M \end{pmatrix} \langle I \| Q_k \| I \rangle \quad . \qquad (2\text{-}2)$$

The Wigner-coefficient appearing in equation (2-2) vanishes unless $\vec{I}$ and $\vec{k}$ add vectorially to form $\vec{I}$. Thus, the only static multipole moments with non-zero expectation value are the 2^k-pole moments with $k \leq 2I$.

Since equations (2-1) would be difficult to evaluate in any but the simplest nuclei, nuclear models are introduced in order to simplify the problem. Of these, the shell model and the collective model have been particularly successful in explaining observed nuclear properties. The shell model arose from an attempt to explain the existence of the so-called "magic numbers" - that is, nuclei with particularly stable nucleon configurations. The collective model was introduced to explain large observed electric quadrupole moments and since then has been developed to explain the well-developed rotational band structure observed in

certain mass regions ($A \sim 25$, $150 < A < 190$, and $A > 225$). These two models, with particular emphasis on the former, will be discussed in the following sections.

1. The Shell Model

The existence of the "magic number" nuclei suggested a nuclear shell structure similar to that found in the electronic structure of atoms. Some, but not all, of the magic numbers could be reproduced if it was assumed that each nucleon moved in a static central potential. This central potential represented the average interaction of the nucleon with the remaining nucleons of the nucleus.

Mayer (Mayer, 1948) and, independently, Haxel, Jensen and Suess (Haxel et al, 1948) proposed the introduction of a spin-orbit force in addition to the central potential. With this extreme single particle model, as it is called, it was found that the magic numbers could be reproduced with a proper choice of the relative strengths of the two interactions. This model also assumed that the internucleon interaction is such that an even number of like nucleons in a given level couple to spin zero. With this assumption, the model predicted that even-even nuclei would have spin zero. This is observed experimentally. The ground state of an odd-mass nucleus is predicted to have the spin and parity of the odd nucleon. With a few exceptions, this is also observed experimentally.

Mayer also introduced the concept of "pairing energy" for like nucleons in the same orbital (Mayer, 1950). The idea is that, when paired off to spin zero, two nucleons in a given level gain a negative pairing energy which increases with the angular momentum of the level. It may then be energetically favourable to pair off nucleons in a higher angular

momentum state at the expense of raising a nucleon from an energetically lower level of lower angular momentum. With the introduction of pairing energy, the non-occurrence of the high spin ground state that are predicted by the shell model can be understood. The level of high spin may be expected to still lie close to the ground state, and, thus, long-lived isomeric states will occur when regions of high spin are being filled.

It should be noted that a level of total angular momentum j can contain 2j+1 like nucleons. Further, for spin purposes, an n-hole configuration, that is, a shell containing 2j+1-n like particles, is treated the same as a configuration of n particles.

No prediction of the spin of odd-odd nuclei can be made by the simple shell model since there is some ambiguity as to the manner in which the angular momenta of the odd nucleons should couple. Nordheim and, more recently, Brennan and Bernstein, have proposed empirical coupling schemes for the determination of the ground state spins of odd-odd nuclei (Nordheim, 1951; Brennan and Bernstein, 1960). If j_1 and j_2 are the angular momenta of the odd-proton and odd-neutron respectively, the Nordheim coupling rules, as modified by Brennan and Bernstein, are as follows: For configurations in which the odd nucleons are both particles or both holes,

(1) $I = |j_1 - j_2|$ or $I = j_1 + j_2$ for $j_1 = \ell_1 \pm 1/2$ and $j_2 = \ell_2 \pm 1/2$,

(2) $I = |j_1 - j_2|$ for $j_1 = \ell_1 \pm 1/2$ and $j_2 = \ell_2 \mp 1/2$.

For hole-particle configurations

(3) $I = j_1 + j_2 - 1$

If one of j_1 or j_2 is 1/2, rule (1) is replaced by

$$(1') \quad I = j_1 + j_2 .$$

The shell model predicts that the magnetic moment of a nucleus with an odd nucleon will be

$$\mu = g_I I = \frac{I}{2} \left[(g_\ell + g_s) + (g_\ell - g_s) \frac{\ell(\ell+1) - 3/4}{I(I+1)} \right] \qquad (2\text{-}3)$$

where $I = \ell \pm 1/2$ is the total angular momentum and g_ℓ and g_s are the orbital and spin g-factors of the odd nucleon. A plot of μ against I using the g-factors of the free nucleon, that is, $g_\ell = 1$ and $g_s = 5.587$ for a proton and $g_\ell = 0$ and $g_s = -3.826$ for a neutron, yields a Schmidt diagram (Schmidt, 1937). With few exceptions, all observed moments lie between the Schmidt lines. Most experimental values, however, lie closer to one Schmidt line than the other. From this correspondence, the parity of the ground state may be inferred.

If all the nuclear angular momentum is assigned to the odd proton and odd neutron, an odd-odd nucleus is predicted to have a nuclear magnetic moment given by

$$\mu_{o\text{-}o} = \frac{I}{2} \left[(g_1 + g_2) + (g_1 - g_2) \frac{j_1(j_1+1) - j_2(j_2+1)}{I(I+1)} \right] . \qquad (2\text{-}4)$$

In this expression, the proton and neutron angular momenta, j_1 and j_2, respectively, couple to a state of total angular momentum I. The proton and neutron g-factors are g_1 and g_2 respectively. It is found that better agreement with experiment is obtained if the g-values of neighbouring odd-even and even-odd nuclei are used in expression (2-4).

The extreme single particle model is an obvious oversimplification since internucleon forces are not taken into account. In particular,

in some nuclei low-lying states with angular momentum coupling of the type $(j)^n_{j-1}$ with n = 3, 5, 7 is found. This coupling cannot be explained by the simple shell model. Kurath has pointed out, however, that a finite range nuclear force can produce low-lying states of this type (Kurath, 1950). In the event that unconventional coupling occurs, however, the shell model predicts that the magnetic moment will be

$$\mu(j^n)_I = \frac{I}{j}\mu(j) \quad . \tag{2-5}$$

In equation (2-5), $\mu(j^n)_I$ is the magnetic moment of a configuration of n particles (or holes) of angular momentum j coupled to total angular momentum I. The shell model prediction for the magnetic moment of a single j nucleon state is $\mu(j)$. This expression follows from the consideration that the g-factor is the same for all nucleons since they are in the same orbit.

Instead of the extreme single particle model, a more realistic approach assumes that only particles in completely filled shells couple to zero total angular momentum. All particles outside this "core" are then considered to move in a potential which consists of a particle-core interaction, a particle-spin-orbit interaction, and a residual particle-particle interaction. The latter is assumed small and is treated as a perturbation. This description leads to the mixing of states of the same orbital angular momentum and parity, particularly the spin-orbit partner. The magnetic moment is especially sensitive to such admixture. Qualitative account of the magnetic moment deviations from the extreme single particle model can be made with this configuration mixing approach (Blin-Stoyle and Perks, 1954; Arima and Horie, 1954).

The individual particle model is an attempt to describe nuclear

properties in terms of single particle states. An energy matrix is set up using wave functions formed from single particle states. This matrix is then diagonalized. The concepts of seniority and isospin are used to identify the low-lying states. Although difficult, this approach has been applied with success to light nuclei ($A < 40$) using a central potential with spin-orbit coupling (Elliott and Lane, 1957).

2. The Collective Model

It is expected that the equilibrium shape of nuclei in the region of closed shells will be approximately spherical. Thus, the nucleons move in an approximately spherical potential and the shell model will give a reasonable description of such nuclei. Far from closed shells, however, it is possible that the effect of the "loose" nucleons will be sufficiently large so that the nucleus will find it energetically favourable to take up a non-spherical equilibrium shape. There can be collective oscillations about the equilibrium shape. Since these oscillations will modify the effective potential in which the loose nucleons move, the motion of these nucleons will be affected more and more as the deformation of the nucleus increases.

Experimental evidence of such collective motion is found in many nuclei. In some mass regions, excited states are spaced in energy in a way similar to the rotational band structure of molecules. Elsewhere, almost equally spaced energy levels are found which are similar to molecular vibrational spectra. These effects, together with the experimental evidence of large positive quadrupole moments and high E2 transition probabilities, imply the cooperative effect of many nucleons. Such correlations could arise from residual long-range effects of the nucleon

force.

This model was developed in detail by Bohr, and was extended and generalized by Bohr and Mottleson (Bohr, 1952; Bohr and Mottleson, 1953). Their description is usually considered in the two extremes of weak and strong particle-core coupling. For the strong coupling case, Nilsson has developed wave functions for an axially symmetric potential. These wave functions are linear combinations of the solutions which occur for the more familiar spherical harmonic oscillator (Nilsson, 1955). Davydov and Filippov (1958) have considered the still more general case of a non-axial nucleus.

The weak coupling case applies to nuclei in regions not far removed from closed shells. Here, the deformation is small and the nuclear shape is approximately spherical. The particle-core interaction is then treated by perturbation theory and has the same effect as configuration mixing in the shell model. Particle states of the same parity and differing in angular momentum by not more than two units are coupled together. In particular, the two spin-orbit partners become mixed.

The strong coupling approximation is used in regions where large deformations are expected, that is, far from closed shells. Usually, an axially symmetric potential is used, and the Hamiltonian is separated into rotational and vibrational parts as well as a part corresponding to particle excitations. The individual particles can then couple separately to the symmetry axis in states specified by their component of angular momentum along this axis. Because of the axial symmetry, configurations of the type $(j)^3_{j-1}$ will arise quite naturally.

The collective model gives reasonable agreement with experimental

results for deformed nuclei. However, the mechanism of distortion is not explained. Furthermore, an adequate description of the transition between weak and strong coupling is not given. It would be expected that particle-core coupling would gradually increase as more extra-core particles are added. Thus, the transition from weak to strong coupling should occur gradually. It is found experimentally, however, that the change is abrupt and occurs within a few mass numbers.

This effect can be explained by the addition of a short-range pairing force which couples pairs of nucleons which are identical in all respects except for their spin projection. These are called "quasi-particle" pairs and the theory is analogous to the pairing theory of superconductivity (Bardeen, Cooper and Schrieffer, 1957). The pairing force favours a spherical nucleus, whereas the long-range forces favour a deformed state. Belyaev shows that, with the addition of the pairing force, a small change in the number of particles in an unfilled shell can produce an abrupt change in the equilibrium deformation (Belyaev, 1959). Similar studies by Kisslinger and others, applied to regions where the shell model is applicable, show that magnetic moments which agree with experiment can be calculated (Kisslinger and Sorensen, 1960; Kisslinger and Freed, 1961).

CHAPTER III

THEORY OF THE EXPERIMENT

Atomic beam experiments are performed at sufficiently low pressures that the atoms are essentially isolated from each other; in fact, the mean free path for collisions is greater than the length of the apparatus. Thus, in the absence of external electromagnetic fields, the atomic Hamiltonian consists of terms internal to an individual atom. This atomic Hamiltonian may be written as

$$\mathcal{H}_{\text{atomic}} = \mathcal{H}_{\text{nuclear}} + \mathcal{H}_{\text{electronic}} + \mathcal{H}_{\text{hyperfine}} . \qquad (3\text{-}1)$$

The quantity $\mathcal{H}_{\text{nuclear}}$ represents the internal energy of the nucleus. Since nuclear energy levels are widely spaced relative to electronic energy levels, the nucleus can be considered to be in a single eigenstate of $\mathcal{H}_{\text{nuclear}}$ characterized by the nuclear spin I. In the following discussion, therefore, this term need not be considered.

The second term, $\mathcal{H}_{\text{electronic}}$, describes the interaction of the atomic electrons moving in the central Coulomb field of a point nucleus. This part of the atomic Hamiltonian contains terms arising from the kinetic energy of the electrons, from the electrostatic interaction of the electrons with the nucleus and with each other, and from the magnetic interaction of the electrons with each other through their spin and orbital magnetic moments. From $\mathcal{H}_{\text{electronic}}$ emerge the gross and fine structure features of the atomic spectrum.

The third term of equation (3-1), $\mathcal{H}_{\text{hyperfine}}$, represents the electric and magnetic interactions of the nucleus with the electrons exclusive of

the Coulomb attraction included in $\mathcal{H}_{electronic}$. $\mathcal{H}_{hyperfine}$ yields the hyperfine structure of the atomic spectrum. It is this term of $\mathcal{H}_{atomic}$ which is of interest in the theory of atomic beam research.

1. The Hyperfine Interaction

In Chapter II, the nuclear multipole operators were written as spherical tensors. The hyperfine interaction may be expressed, therefore, as a sum over k of the product of two tensor operators of order k (Schwartz, 1955):

$$\mathcal{H}_{hyperfine} = \sum_{k} \vec{T}^{k}(e) \cdot \vec{T}^{k}(n) \qquad (3\text{-}2)$$

Here $\vec{T}^{k}(e)$ and $\vec{T}^{k}(n)$ are irreducible tensors operating in the electronic system and in the nuclear system respectively. With this formalism, it can be shown that the highest value of k that can occur in the expansion (3-2) is the lesser of 2I and 2J, where I and J are the nuclear and total electronic angular momenta respectively.

Since the work described here pertains only to atoms in the $^{2}S_{\frac{1}{2}}$ electronic state, only the magnetic dipole interaction is non-zero. In this case, it is more convenient to write the interaction in the form

$$\mathcal{H}_{hyperfine}(M1) = -\vec{\mu}_I \cdot \vec{H}_J(0) \qquad (3\text{-}3)$$

where $\vec{H}_J(0)$ is the magnetic field produced by the electrons at the position of the nucleus. The nucleus has been assumed a point dipole moment in writing equation (3-3).

The nuclear moment, $\vec{\mu}_I$, can be related to the nuclear spin, $\vec{I}$, by the equation

$$\vec{\mu}_I = g_I \mu_o \vec{I} \qquad (3\text{-}4)$$

where μ_o is the Bohr magneton and g_I is the nuclear g-factor. Similarly

the atomic magnetic moment, $\vec{\mu}_J$, can be related to the total electronic angular momentum, $\vec{J}$, by the equation

$$\vec{\mu}_J = g_J \mu_o \vec{J} \tag{3-5}$$

where g_J is the electronic g-factor. Since $\vec{H}_J(0)$ has the direction of $\vec{J}$, then equation (3-3) can be rewritten as

$$\mathcal{H}_{\text{hyperfine}}\,(M1) = ha\,\vec{I}\cdot\vec{J} \tag{3-6}$$

where a , the magnetic dipole interation constant, contains all the proportionality constants. Explicitly,

$$ha = -\left(\frac{\mu_I}{I}\right)\frac{\vec{H}_J(0)\cdot\vec{J}}{\vec{J}\cdot\vec{J}} \tag{3-7}$$

and a has the units of frequency. Fermi (Fermi, 1930) has calculated the field $\vec{H}_J(0)$ at a point nucleus to be

$$\vec{H}_J(0) = \frac{8\pi}{3} g_J \mu_o \left|\Psi(0)\right|^2 \vec{J} \tag{3-8}$$

where $\Psi(0)$ is the wave function of the s-electron at the nucleus. By combining equations (3-7) and (3-8), the magnetic dipole interaction constant can be written as

$$ha = \frac{-8\pi}{3}\,\frac{\mu_I}{I}\,g_J \mu_o \left|\Psi(0)\right|^2 \tag{3-9}$$

The ratio of the interaction constants of two isotopes of the same element yields the Fermi-Segrè equation

$$\frac{a_1}{a_2} = \left(\frac{\mu_I}{I}\right)_1 \Big/ \left(\frac{\mu_I}{I}\right)_2 \tag{3-10}$$

since the electronic factors cancel.

Experimentally, however, it has been found that equation (3-10) is not quite valid, and equation (3-10) is properly written

$$\frac{a_1}{a_2} = \left[\left(\frac{\mu_I}{I}\right)_1 \Big/ \left(\frac{\mu_I}{I}\right)_2\right](1 + {}_1\Delta_2) \cdot \qquad (3\text{-}11)$$

By convention, isotope one is the lighter isotope. In equation (3-11), ${}_1\Delta_2$ is called the hyperfine structure anomaly. This anomaly arises because of the finite size of the nucleus. Since the electron wave function varies over the nucleus, the hyperfine interaction constant is sensitive to the distribution of nuclear magnetism. The hyperfine interaction would then be expected to be reduced by a small amount ϵ from that calculated for a point dipole (PD). Taking into account the finite size of the nucleus, equation (3-10) is written

$$\frac{a_1}{a_2} = \left(\frac{a_1}{a_2}\right)_{PD} \cdot \frac{(1+\epsilon_1)}{(1+\epsilon_2)}$$

which leads directly to equation (3-11) if terms of order ϵ^2 are neglected and ${}_1\Delta_2$ is defined as

$${}_1\Delta_2 = \epsilon_1 - \epsilon_2 \cdot$$

Bohr and Weisskopf have developed a theory for the calculation of ϵ which is applicable to heavy nuclei (Bohr, 1950). This theory has been extended by Bohr (Bohr, 1951a; Bohr, 1951b), Eisinger and Jaccarino (Eisinger and Jaccarino, 1958), and Stroke (Stroke, 1959). More recently, Stroke and Blin-Stoyle have considered the effect of configuration mixing on the hyperfine structure anomaly (Stroke and Blin-Stoyle, 1961). It is not, however, the purpose of this work to pursue the point any further.

The interaction constant a can be simply related to the spacing of the zero-field hyperfine energy levels. In the $|IJFM>$ representation, in which the nuclear spin $\vec{I}$ is coupled with the electronic angular momentum $\vec{J}$ to form a state of total angular momentum $\vec{F}$, with projection M on the quantization axis, the interaction energy is obtained by taking the diagonal elements of the interaction Hamiltonian. Thus,

$$W_{M1}(F) = \langle IJFM | \mathcal{H}_{hyperfine}\ (M1) | IJFM \rangle$$

$$= ha \langle IJFM | \vec{I}\cdot\vec{J} | IJFM \rangle$$

$$= \frac{ha}{2}\left[F(F+1) - I(I+1) - J(J+1)\right] \quad . \qquad (3\text{-}12)$$

From equation (3-12), the separation between the two hyperfine levels is given by

$$\Delta W = h\Delta\nu = \left|W_{M1}\ (F = I+\tfrac{1}{2}) - W_{M1}\ (F = I-\tfrac{1}{2})\right|$$

$$= \frac{h}{2}\ (2I + 1)\ |\ a| \quad . \qquad (3\text{-}13)$$

Equation (3-13) defines the hyperfine separation $\Delta\nu$ which is usually expressed in megacycles per second. Experimental values of $\Delta\nu$ range from zero (for the I = 0 or J = 0 case) to about 50,000 megacycles per second in Ag^{108}.

2. <u>The Hyperfine Interaction in an External Magnetic Field</u>

In the presence of an external magnetic field, H, the Hamiltonian must include the interaction of the nuclear and electronic magnetic moments with this external field. The Hamiltonian may be written

$$\mathcal{H} = \mathcal{H}_{hyperfine}\ (M1) - \vec{\mu}_I\cdot\vec{H} - \vec{\mu}_J\cdot\vec{H}$$

$$= ha\,\vec{I}\cdot\vec{J} - g_I\mu_o\,\vec{I}\cdot\vec{H} - g_J\mu_o\,\vec{J}\cdot\vec{H} \quad . \qquad (3\text{-}14)$$

The representation in which the expectation value of $\mathcal{H}$ is found depends upon the relative size of the first and third terms (the second is three orders of magnitude smaller than the third unless J = 0).

For small values of H, coupling between I and J is much stronger than coupling between J and H. In this case, off-diagonal matrix elements in F may be neglected and the $|FM\rangle$ representation is most convenient. The resulting expression for the interaction energy is

$$W(F,M) = \langle FM|\mathcal{H}|FM\rangle$$

$$= \frac{ha}{2}\left[F(F+1) - I(I+1) - J(J+1)\right] - g_F \mu_o H M \qquad (3\text{-}15)$$

where

$$2F(F+1)g_F = g_J\left[F(F+1) + J(J+1) - I(I+1)\right] + g_I\left[F(F+1) + I(I+1) - J(J+1)\right]$$

$$\approx g_J\left[F(F+1) + J(J+1) - I(I+1)\right] \quad . \qquad (3\text{-}16)$$

Thus, in a weak field, the state with energy W(F) breaks into 2F + 1 equally spaced energy levels with spacings given by

$$\frac{W(F = I\pm\frac{1}{2},M) - W(F = I\pm\frac{1}{2}, M-1)}{h} = \mp g_J \frac{\mu_o H}{(2I+1)h} \simeq \pm 2.8 \frac{H}{2I+1} \text{ Mc/sec.} \qquad (3\text{-}17)$$

In writing equation (3-17), the g_I term has been dropped as in equation (3-16) and $g_J(^2S_{\frac{1}{2}})$ has been put equal to -2. Transitions between these levels are called Zeeman transitions.

For values of H large enough so that the coupling between J and H is much stronger than the coupling between I and J, it is more convenient to use the $|M_I M_J\rangle$ representation. Here, M_I and M_J are the projections of I and J respectively upon the field direction. The energy of the state $|M_I M_J\rangle$ is then given by

$$W(M_I M_J) = \langle M_I M_J |\mathcal{H}| M_I M_J\rangle$$

$$= ha\, M_I M_J - g_I \mu_o M_I H - g_J \mu_o M_J H. \qquad (3\text{-}18)$$

When I and J are decoupled the atom is said to be in the Paschen-Back region. Here, ignoring the term in g_I, there are 2J+1 sets of 2I+1 equally spaced levels of separation $2|M_J|h\Delta\nu/(2I+1)$.

The intermediate field region, that is, the region in which the energy ha is comparable to $\mu_o H$, is more complicated. For a general case, a determinant must be set up, but, in the case of $J = \frac{1}{2}$, an analytic expression for the energy may be obtained using either representation (Breit and Rabi, 1931; Ramsey, 1956). The expression, known as the Breit-Rabi equation, can be written

$$W(F,M) = \frac{-h\Delta\nu}{2(2I+1)} - \frac{\mu_I}{I}\mu_o HM \pm \frac{h\Delta\nu}{2}\left[1 + \frac{4M}{2I+1}x + x^2\right]^{\frac{1}{2}} \qquad (3\text{-}19)$$

where $\Delta\nu$ is the hyperfine separation of equation (3-13) and x is a dimensionless parameter defined by

$$x = \left|\left(\frac{\mu_I}{I} - 2\mu_J\right)\frac{\mu_o H}{h\Delta\nu}\right| \quad . \qquad (3\text{-}20)$$

The sign of the radical in equation (3-19) is to be taken positive for the $F = I+\frac{1}{2}$ state and negative for the $F = I-\frac{1}{2}$ state.

If the energy in units of $h\Delta\nu$ is plotted against x, one obtains what is known as a Breit-Rabi diagram. Figure 1 is an example of such a diagram for the case of I = 7/2 and positive nuclear moment. These diagrams, showing the behaviour of the energy levels as a function of magnetic field, are often used to show the transitions observed in an atomic beam experiment.

3. The "Flop-In" and "Flop-Out" Techniques

In an atomic beam experiment, a beam of atoms passes, in succession, through a region of inhomogeneous magnetic field (A field), a region of homogeneous field (C field), and another region of inhomogeneous field (B field). An atom with a magnetic moment, $\vec{\mu}$, experiences a deflecting

FIGURE 1

Energy levels for $I = 7/2$, $J = 1/2$, and $\mu_I > 0$.

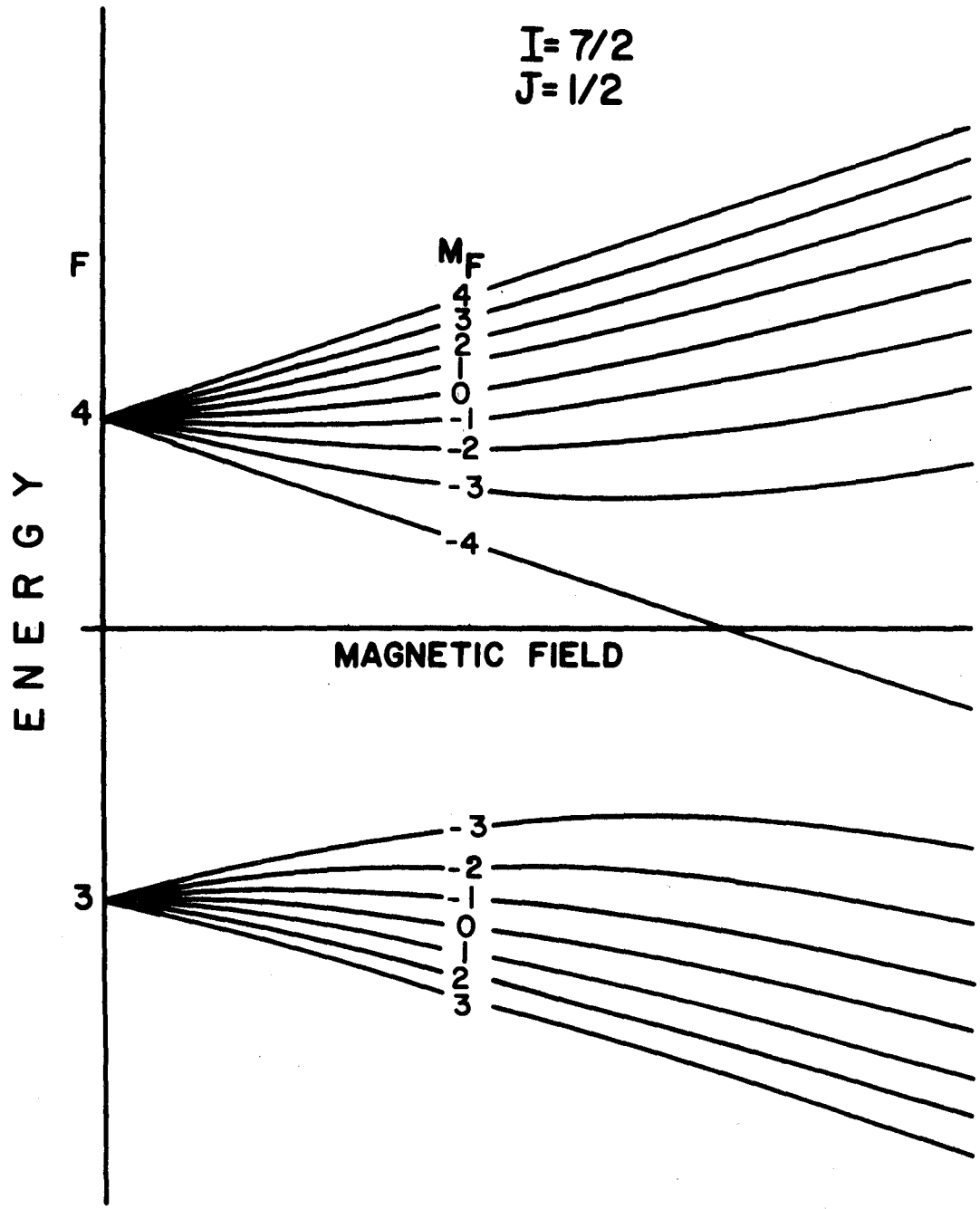
I= 7/2
J= 1/2
F
M_F
4
3
2
1
0
-1
-2
-3
-4
4
3
-3
-2
-1
0
1
2
3
ENERGY
MAGNETIC FIELD

force in the inhomogeneous field regions given by

$$\vec{F} = -\nabla W = -\frac{\partial W}{\partial H}\nabla H = +\mu_{eff}\nabla H \quad . \qquad (3\text{-}21)$$

In the homogeneous field region, transitions are induced between magnetic substates of the atom by a weak radio-frequency oscillating field. It can be shown that the atoms will be refocussed at a detector on the axis of the machine provided that the following condition is satisfied (Ramsey, 1956)

$$\frac{H_A}{H_B} = k\left[\frac{(\mu_{eff})_B}{(\mu_{eff})_A}\right] \quad . \qquad (3\text{-}22)$$

Subscripts A and B refer to quantities measured in the A and B field regions respectively. The constant k depends upon machine dimensions and can be positive or negative depending upon the relative directions of the field gradients. The value of μ_{eff}, which can also be positive or negative, depends on the quantum state of the atom and on the magnitude of the field.

Since the deflecting fields in an atomic beam apparatus are usually 10 kilogauss or more, which is generally sufficient to completely decouple $\vec{I}$ and $\vec{J}$, the effective moments are to be found in the Paschen-Back region. Neglecting the term in g_I in equation (3-18), it follows that there will be 2J+1 different values of μ_{eff} corresponding to the different M_J. For J=1/2, then, there are two kinds of atoms - those with positive effective moment and those with negative effective moment. In weaker deflecting fields, however, each state $|FM\rangle$ has a different value which is field dependent. This may be understood by referring to Figure 1, noting that the effective moment is given by the slope of a curve at the appropriate value of x.

A flop-out machine is designed so that atoms will be focussed at the detector if they do not undergo a transition. Assuming that the two

deflecting fields are equally strong, this would occur for a geometry such that k = +1. If a transition does occur that changes μ_{eff} appreciably, then the focussing condition will be violated for those atoms and the intensity of the beam reaching the detector will diminish. Transitions between states which have effective moments of opposite sign would certainly be detectable. If the deflecting fields are not too strong, however, then the occurrence of any allowed transition will reduce the detector signal.

Conversely, in a flop-in machine, k is negative. Only atoms which undergo transitions between states whose effective moments have opposite sign can reach the detector causing an increase in beam intensity on resonance. That the condition being sought gives an increase at the detector, rather than a decrease, is an advantage in an experiment involving radioactive atoms and, hence, counting statistics. The flop-in machine does have the disadvantage, however, that the number of observable transitions is reduced.

The machine used for these experiments was of the flop-in type. As will be described below, however, the deflecting magnetic fields were not strong enough to decouple $\vec{I}$ and $\vec{J}$ in the case of Ag^{109m}. This inadvertent novelty was both a nuisance and a boon as many unconventional transitions were observed.

4. Allowed Transitions

Because the transitions to be induced in the region between the deflecting magnets involve states of the same parity, the selection rules are those for magnetic dipole radiation. If the C field is weak, these

selection rules are:

$$\Delta F = \pm 1 \qquad \Delta M = 0 \qquad (\sigma \text{ - transitions})$$

$$\Delta F = 0, \pm 1 \qquad \Delta M = \pm 1 \qquad (\pi \text{ - transitions}).$$

To induce a σ-transition, it is necessary to have a component of the oscillating field directed along the quantization axis provided by the C field. For a π-transition, a component at right angles is necessary.

If the oscillating field is relatively weak, the transition frequency between states with energy $W(F,M)$ and $W(F',M')$ is given by the Bohr condition

$$h\nu_o = \left| W(F,M) - W(F',M') \right| .$$

Because the perturbation is applied for only a finite time duration depending on the velocity v of each individual atom, the resonance is not infinitely sharp. For the case of a constant r.f. amplitude over a region of length ℓ, Rabi (1937) has shown that the transition probability is maximum for $\nu = \nu_o$. The full width at half maximum is of the order of $\bar{v}/\ell$. Very often, σ-transitions are induced by a r.f. loop for which the field in the first half of the r.f. region is 180° out of phase with that in the latter half. In that event, the appropriate expression for the transition probability has a minimum at $\nu = \nu_o$, and peaks appear on either side at $\nu - \nu_o \approx \pm \bar{v}/\ell$.

Transitions violating these selection rules can also be induced if the strength of the oscillating field is sufficiently large. Several authors (Hack, 1956; Salwen, 1956) have investigated the theory of these multiple quantum transitions. The probability of a transition in which n photons are successively absorbed can be appreciable if there are real intermediate states at essentially the appropriate spacing. They are

commonly seen in practice, therefore, for the case of a π-loop and a relatively weak static field so that the energy levels are given approximately by equation (3-15). Their selection rule is

$$\Delta F = 0 \qquad \Delta M = \pm n \ .$$

The resonance shape for these differs in two important ways from that of a normal one quantum transition. The full width at half maximum is reduced by a factor 1/n and becomes less still when the intermediate states are not equally spaced. The peak height depends very sensitively on the spacing of the intermediate states and is less, other things being equal, the higher the multiplicity. Thus, a n-quantum transition may be distinguished by the fact that, as one follows it to higher field, the line becomes progressively narrower and less intense relative to a normal transition. There is one other feature of a multiple quantum resonance which is important. The transition probability is a maximum for a frequency satisfying a generalized Bohr condition

$$h\nu_o = \frac{1}{n} \left| W(F,M) - W(F',M') \right| + \epsilon \qquad (3\text{-}23)$$

where ϵ represents a power shift which may be significant depending on the r.f. field strength. Salwen (1956) gives an expression for ϵ based on an approximate solution to the problem.

Allowed transitions can be classified, then, into two general groupings - the so-called hyperfine transitions with $\Delta F = \pm 1$ which are invariably single quantum in nature, and the Zeeman transitions with $\Delta F = 0$, $\Delta M = \pm n$ ($n = 1, 2, \ldots$) which may occur within the F multiplets.

For a $J = 1/2$ atom in a flop-in machine with deflecting fields operating at large x, the observable allowed transitions include, therefore, a group of hyperfine transitions (both σ and π) whose frequencies

are of the order of $\Delta\nu$ and approach that limit for zero field. In addition, there will be a group of Zeeman transitions (π type) in the multiplet $F = I + 1/2$ between the state $|I + 1/2, \pm (I + 1/2)\rangle$ and the other states $|(I + 1/2), \pm (I + 1/2-n)\rangle$. The choice of sign is determined by the sign of the dipole interaction constant, the upper sign corresponding to negative a. This second set of transitions becomes degenerate in the weak field limit and approaches zero frequency at zero field. No other transition satisfies both the selection rules and the condition for observability, namely that the high field effective moment must change sign.

5. The Determination of Atomic and Nuclear Properties

In principle, any set of N measured transition frequencies, either of a different type at one field or of the same type at various fields or both, could be fitted to a Hamiltonian containing N empirical coefficients. But, based on the foregoing considerations and on the practical necessity of having some idea of the frequency range in which a sought after transition is to be found, there is a preferred method of approach to the experimental determination of the constants J, I, g_J, g_I, a, (b)*, and (c)* which characterize the Hamiltonian. Also, because of the finite line width, which may be increased due to the presence of unavoidable C field inhomogeneities, certain transitions and certain fields must be chosen in order to minimize the errors in the determination. In the following brief account, it will be assumed that $J = 1/2$ since that is the case for the atoms under study. More complete details, including the effect of b and c,

---

* b and c denote the electric quadrupole and magnetic octupole interaction constants, respectively, which may appear when $J \neq 1/2$.

may be found in Ramsey and Kopfermann (Ramsey, 1956; Kopfermann, 1958). The detailed study of samarium-153 by Eastwood considers these interactions in detail (Eastwood, 1964).

a) The Electronic Gyromagnetic Ratio (g_J)

Values of g_J, at least to low precision, are known for most atomic ground states. Interest in determining them to high precision is due, in part, to the fact that small admixtures in the electronic wave function can then be determined.

The most convenient way of determining g_J is to study a stable isotope with $I = 0$ if it is available. In that event, all terms in the Hamiltonian (3-14) are zero except the last one. A direct determination of g_J can then be made from the frequency of the Zeeman single resonance if the field is known. When $I \neq 0$, one can still study the Zeeman transitions, but only in a very strong magnetic field is the analysis direct (the practical selection rules are $\Delta M_J = \pm 1$, $\Delta M_I = 0$, since there is little possibility of flipping the small nuclear moment). Then, by equation (3-18), there will be a sequence of equally spaced π-lines whose frequences depend linearly on H and are a direct measure of g_J.

b) The Nuclear Spin (I)

The spin of a nucleus is determined in an atomic beam experiment by observing Zeeman transitions in a low magnetic field. Equation (3-17) can be applied yielding the resonance frequency.

$$\nu = \frac{-g_J}{2I+1}\left(\frac{\mu_o H}{h}\right) \quad . \qquad (3\text{-}17)$$

If the electronic g-factor is known for the element to be studied, the

spin of the nucleus follows unambiguously from the resonant frequency and the value of the magnetic field. For $J \neq 1/2$, a somewhat different expression is obtained, but the principle of the nuclear spin being determined by the frequency of the low-field Zeeman transitions still holds.

c) The Magnetic Dipole Interaction Constant (a)

The usual method of determining a is to observe the transition $(F = I + 1/2, M = -F) \longleftrightarrow (F = I + 1/2, M = -F + 1)$ as the magnetic field H is increased. Provided that $x \propto H/a$ is small, the frequency of this transition may be expressed as a power series in H. The deviation of the observed transition frequency from the frequency given by equation (3-17) is then a measure of the hyperfine separation. One can, in this way, continue to increase the magnetic field H until the hyperfine separation is determined as accurately as desired. Of course, the exact Hamiltonian expression, and not the power series expansion, is used. A value of g_I, at least approximately correct, may be determined using equations (3-13) and (3-10). This value of g_I can then be inserted into the expression for the transition frequency and the hyperfine separation recalculated. This continues until values of a and g_I are consistent. If there is actually a significant hyperfine structure anomaly and g_I is sizeable, this procedure will lead to an erroneous value for a.

Alternately, or as well, one can look for the direct hyperfine transitions. These transitions occur at much higher frequencies ($\approx \Delta\nu$) than the Zeeman transitions. This procedure is only practical after the hyperfine separation has already been determined to sufficient accuracy to restrict the search to a reasonable frequency range, that is, a few megacycles at most. Of course, this procedure also requires the avail-

ability of r.f. equipment at the frequency involved. If the hyperfine separation is very large, this may not be a pleasant prospect.

d) The Nuclear Gyromagnetic Ratio (g_I) and Dipole Moment ($\mu_I = Ig_I$)

In units of Bohr magnetons, $|g_I| \lesssim 10^{-3} |g_J|$. Accordingly, the g_I term in equation (3-14) is always very small compared to the g_J term. Since both depend on the magnetic field in the same manner, nothing can be done to emphasize the effect of the term to be measured. There is something to be gained, however, by making the observation under the most advantageous experimental circumstances. For the case $J = 1/2$ and $I \geq 1$, there exists a non-zero field for which the two hyperfine transitions

$$(I + 1/2, -I + 3/2) \longleftrightarrow (I - 1/2, -I + 1/2)$$

and

$$(I + 1/2, -I + 1/2) \longleftrightarrow (I - 1/2, -I + 3/2)$$

are field independent, that is, the frequencies do not depend to first order on H. At this field, therefore, these lines will be especially narrow since magnetic field inhomogeneities do not cause any broadening. From equation (3-19) it follows that the difference between them is simply $2 g_I \mu_o H/h$. Of course, each transition has a frequency of the order of the hyperfine separation, so that, if the hyperfine separation is large, a high frequency experiment would be necessary. Failing this, or in the case of $I = 1/2$, the best that can be done is to determine the frequency of a Zeeman transition to as high accuracy as possible and extract g_I using previous knowledge of the precision g_J.

Failing a direct measurement of g_I in this way, the nuclear magnetic moment must be inferred from a using the Fermi-Segrè formula (equation (3-10)) and a comparison isotope for which μ_I is known. Because of the possibility of a large hyperfine anomaly in $^2S_{1/2}$ atoms and of a

lesser one in $^2P_{1/2}$ states, the accuracy of this approach is limited to about one percent. For other atomic states where $J > 1/2$, anomalies will be small and the use of the Fermi-Segrè formula is common.

6. Unusual Transitions in the Flop-In Method

The foregoing discussion has considered the flop-in method using deflecting fields which operate at large x. If weaker fields are used, or, what amounts to the same thing, an atom with a particularly large hyperfine separation is being studied, additional transitions may become observable just as in the case of the flop-out method. If the two deflecting fields operate at different fields, and, hence, different x, then an even more novel situation can prevail.

The deflecting magnets in the machine with which these experiments were performed are designed such that proper focussing occurs when the strength of the A field is about one-half that of the B field. In the studies thus far carried out in this laboratory, the isotopes had small enough hyperfine separations so that even the 5 kilogauss A field is operating at a large x *. In the case of Ag^{109m}, however, one can anticipate a large hyperfine separation if the nuclear magnetic dipole moment is greater than 1 or 2 nuclear magnetons because the electronic configuration of silver is $^2S_{1/2}$ which produces a large magnetic field at the nucleus. If the hyperfine separation is large enough so that the operating point of the A magnet (x_A) is much less than unity for the field at which it runs, then transitions from the $F = I + 1/2$, $M = \pm (F - 1)$ state as

---

* This was, perhaps, not the case for the spin measurement of In^{117} (Cameron, 1962), but for a spin measurement the precise operation is of little importance.

well as from the $F = I + 1/2$, $M = \pm F$ state (the upper and lower signs for the case of negative and positive nuclear moments respectively) will be observable. This is illustrated in Figure 2 which is again a Breit-Rabi diagram for the case of $I = 7/2$ and positive nuclear moment. Consider, for example, the situation in which the hyperfine separation and the deflecting fields are such that $x_A \approx 0.3$ and $x_B \approx 0.7$. It might then be possible to focus transitions originating on the $F = 4$, $M = -3$ level and terminating on the $F = 4$, $M = -2, -1, \ldots, +4$ levels. The reverse transitions, that is, transitions in the $F = 4$ multiplet terminating on the $M = -3$ level, would not be favourable, however, because of the small effective moment of the $F = 4$, $M = -3$ level in the second deflecting field.

The effective moment of a level of given M in the $F = 3$ (or, in the general case, $F = I - 1/2$) multiplet differs only in sign from that of the corresponding level in the $F = 4$ (or $F = I + 1/2$) multiplet. Thus, if Zeeman transitions are to be expected originating on the $F = 4$, $M = -3$ level, then corresponding Zeeman transitions in the lower multiplet originating on the $F = 3$, $M = -3$ level should be observable. Since, for the case of $J = 1/2$, the weak field splitting between adjacent substates is the same in both the upper and lower multiplets, these transitions will appear at nominally the same frequency as the others. This may be seen by putting $F = I \pm 1/2$, $J = 1/2$ into equation (3-16).

Furthermore, in this situation, the normally focussable ($F = 4$, $M = -4$) $\longleftrightarrow$ ($F = 4$, $M = -3$) transition would not be observable since the sign of the effective moment does not change for the case where the atom passes through the A magnet in the $M = -3$ state. The reverse situation has already been discarded above. However, multiple quantum transitions of the type ($F = 4$, $M = -4$) $\longrightarrow$ ($F = 4$, $M = -4 + n$) with $n \geqslant 2$ might be

FIGURE 2

Possible flop-in transitions for an atom possessing a large hyperfine structure separation. Since I and J are not completely decoupled in the deflecting field regions, transitions not usually seen become focussable. The arrow indicates the direction in which the transition must occur. The vertical lines labelled x_A and x_B are the value of x (equation (3-20)) in the first and second deflecting fields respectively.

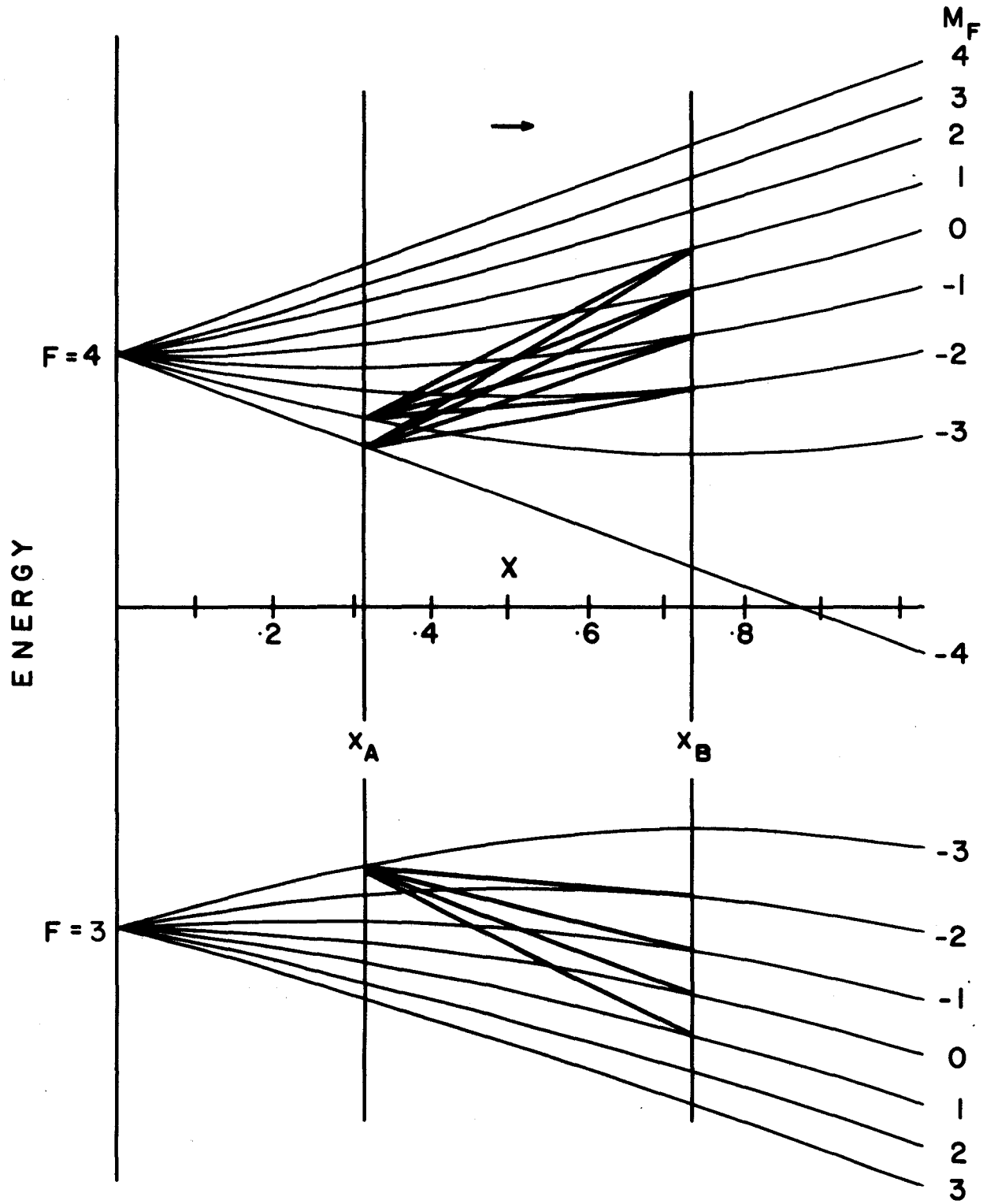
M_F
4
3
2
1
0
-1
-2
-3
-4
F = 4
F = 3
ENERGY
X
·2
·4
·6
·8
X_A
X_B

expected. For $n \gtrsim 5$, the reverse transitions would also be focussable. The arrow, at the top of Figure 2, indicates that, with this just noted exception, all of the transitions discussed would be observable in one-way only.

Depending on the exact value of x_A, it might also be possible to focus transitions originating on the M = -2 states in each multiplet. This feature has no special merit and was not exploited in this work.

For the case of J = 1/2, the frequency of the general n-quantum π-transition between the levels with energy W(F,M) and W(F,M+n) can be obtained from the Breit-Rabi equation (equation (3-19)). In order to simplify notation, n-quantum transitions originating on the (F = I + 1/2, M = -F), (F = I + 1/2, M = -F + 1) and (F = I - 1/2, M = -F) levels will be designated as n, n', and n'' transitions respectively. Similarly, $\nu(n)$, $\nu(n')$, and $\nu(n'')$ will be the frequencies at which these transitions occur. Thus, for example,

$$\nu(n) = \frac{1}{n}\left[\frac{W(F=I+1/2,\ M=-(I+1/2)+n) - W(F=I+1/2,\ M=-(I+1/2))}{h}\right]$$

$$= \frac{1}{n}\left\{-\frac{\mu_I}{I}\frac{\mu_o H n}{h} + \frac{\Delta\nu}{2}\left(\left[1 + \frac{2(2n-(2I+1))}{2I+1}x + x^2\right]^{1/2} - (1-x)\right)\right\}.$$

Since the transitions take place in the C magnet, it is to be noted that, in this expression and in all others in the remainder of this section, x is related to the C magnet field strength and not that of the deflecting magnets.

If x is small enough that the terms in x and x^2 of the radical in the Breit-Rabi equation are considerably less than unity, the radical can be expanded in a power series in x. The frequencies of the multiple quantum transitions may then be obtained by subtracting the expression for the

various energy levels. Defining

$$\nu_N = \left(\frac{-\mu_J}{J} + \frac{\mu_I}{I} \right) \frac{\mu_o H}{(2I+1)h} = \frac{x\Delta\nu}{2I+1} \quad , \tag{3-24}$$

the following expressions, to second order in H, are obtained for $\nu(n)$, $\nu(n')$, and $\nu(n'')$:

$$\nu(n) = \nu_N - \frac{\mu_I}{I} \frac{\mu_o H}{h} + \frac{\nu_N^2}{\Delta\nu} \left[2I+1-n \right] \quad , \tag{3-25}$$

$$\nu(n') = \nu_N - \frac{\mu_I}{I} \frac{\mu_o H}{h} + \frac{\nu_N^2}{\Delta\nu} \left[2I-1-n \right] \quad , \tag{3-26}$$

and

$$\nu(n'') = \nu_N + \frac{\mu_I}{I} \frac{\mu_o H}{h} + \frac{\nu_N^2}{\Delta\nu} \left[2I-1-n \right] \quad . \tag{3-27}$$

In equation (3-25), n takes the values n=1, 2 ..., 2I+1, and in equations (3-26) and (3-27), n takes the values n=1,2 ...2I-1. Comparing equations (3-26) and (3-27) with equation (3-25) it is seen that, to second order in H,

$$\nu(n') = \nu(n+2)$$

and

$$\nu(n'') = \nu(n+2) + 2 \frac{\mu_I}{I} \frac{\mu_o H}{h} \quad .$$

It is further noted, that, for any value of H,

$$\nu(n'') - \nu(n') = 2 \frac{\mu_I}{I} \frac{\mu_o H}{h} \quad . \tag{3-28}$$

The possibility of observing these extra Zeeman transitions means that the analysis of the data is much less straightforward until the observed resonances have been correctly identified. Once the identification is consistent, however, the extra data may be used to overdetermine the parameters of the Hamiltonian. In addition, their multiple quantum nature means that the resonances will be narrower than the conventional Zeeman resonance so that greater accuracy may be achieved at the same field.

There is one particular feature of the extra transitions which may prove to be of considerable value. As noted above, the $n' n''$ transition frequencies differ only by a term proportional to the nuclear magnetic moment. The observation of narrow multiple quantum pairs of this type will lead, therefore, to a direct measurement of the nuclear magnetic moment without the necessity of making the type of measurement indicated previously (which involves frequencies of the order of the hyperfine separation). Of course, the possibility of power shifts as given by equation (3-23) would have to be investigated in detail. Thus, although a power shift might occur, it should be calculable for each, and the difference in frequencies could be corrected accordingly. The use of this procedure, at least to low accuracy, will be demonstrated in the results that follow for Ag^{109m}.

CHAPTER IV

EXPERIMENTAL APPARATUS AND TECHNIQUE

The flop-in atomic beam apparatus used in these experiments has been described in detail elsewhere (King, 1960; Cameron et al, 1962). Since few modifications were made to the machine for the purpose of these experiments, only the general principles of operation and a brief description of construction will be presented here. The discussion will also refer mainly to the study of radioactive isotopes.

1. Principles of Operation

A purely schematic plan of the apparatus is shown in Figure 3. O is an oven into which the material to be studied is placed. This oven is heated to a temperature sufficient to produce a vapour pressure of the source material of between 0.1 and 1.0 millimeters of mercury. The beam of source atoms which is formed streams through a slit 0.005 inches wide into an enclosure in which the pressure is low enough so that gas scattering is effectively eliminated. Defined by vertical slits, the beam passes in succession through these magnets designated the A, C, and B magnets respectively. The A and B magnets produce strong inhomogeneous fields; the C magnet produces a relatively weak uniform magnetic field. The relative directions of these fields and field gradients are indicated in the figure.

Beam definition is obtained by an additional slit at the exit of each of the A and B magnets. By means of slow motion screw drives through rotating vacuum seals in the apparatus base-plate, the position of the

FIGURE 3

A schematic plan of a "flop-in" atomic beam apparatus. The solid line illustrates the trajectory of an atom which has undergone a transition in the C field region such that the focussing conditions are satisfied; the dashed line illustrates the trajectory of an atom for which the focussing conditions are not satisfied. O is the source oven, S is the removable stop and D is the detector. The relative directions of the fields and field gradients are indicated.

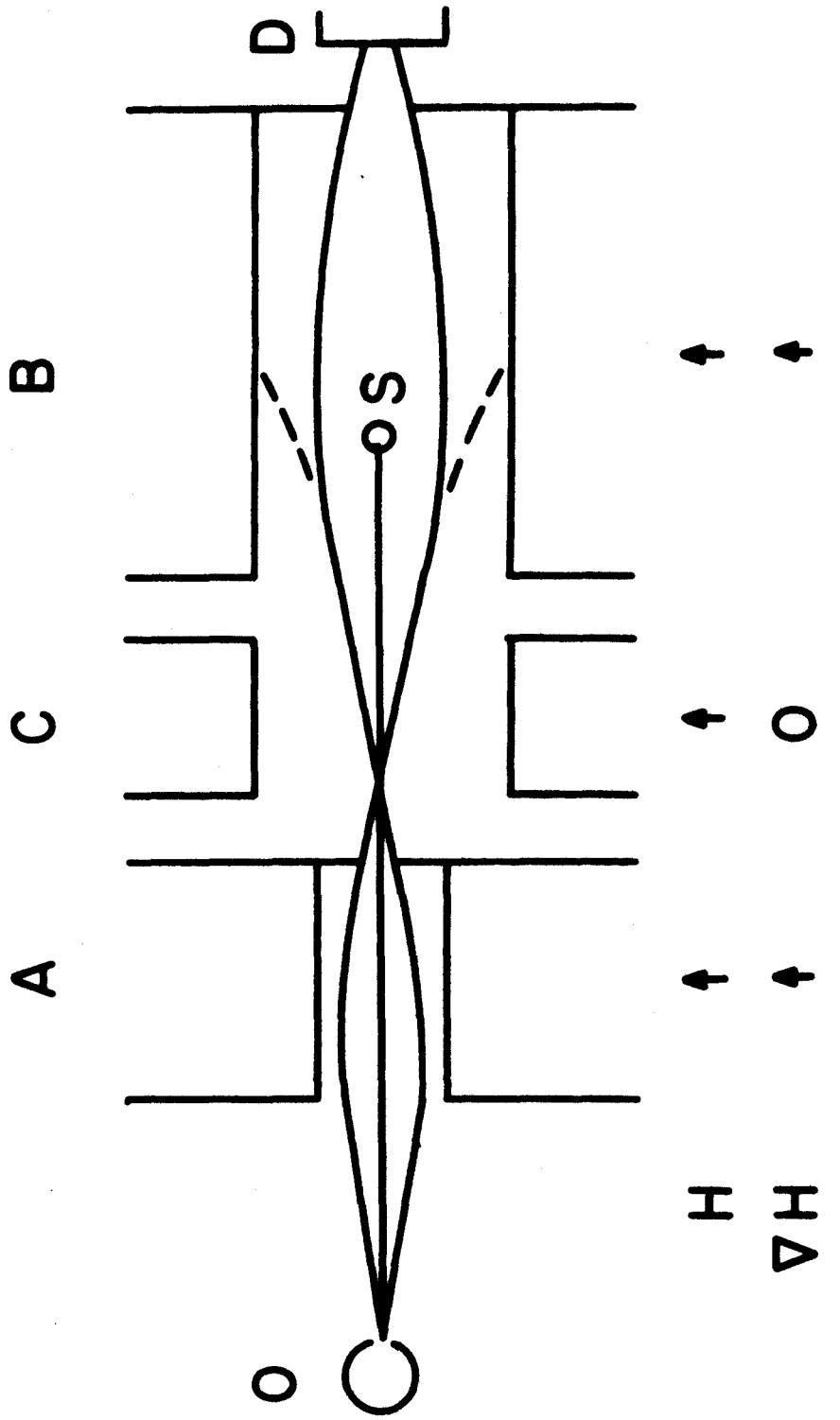
D
B
S
C
O
A
H
H
O

A magnet slit assembly and of each jaw of the B magnet slit may be independently adjusted. The convenience of this latter facility was exploited for Cs^{138} experiments.

A weak oscillating radiofrequency field, produced by a suitable antenna (not shown), is also introduced in the C field region. This oscillating field induces transitions between the magnetic substates of the atom. An atom which undergoes a transition such that the focussing condition (equation(3-22)) is satisfied will be focussed at the detector D. The trajectory of such an atom is illustrated by the solid line in Figure 3. An atom not undergoing such a transition or undergoing no transition at all will not be focussed at the detector. Such an atom is lost from the beam; its trajectory is illustrated by the broken line in Figure 3.

Since some atoms of the beam have sufficient speed that they are undeflected by the magnets, a stop S is placed within the field region of the B magnet at the position of maximum excursion of the resonant atoms. This stop blocks straight line paths from the source to the detector. The stop may, however, be withdrawn to permit alignment of the source.

In actual practice, however, some gas scattering does occur and a non-zero signal is present at the detector at all times. However, when transitions are induced between magnetic substates such that refocussing does occur, the signal at the detector increases. The frequency at which this transition occurs may then be related to nuclear and electronic properties as discussed in Chapter III.

2. The Vacuum System

The vacuum system of this apparatus consists of two welded aluminum cases which are joined by a buffer chamber. Narrow slits in the walls of the buffer chamber allow the beam to pass but restrict gas flow

from the relatively high pressure oven section into the rest of the machine. Each case is separately sealed to the same heavy duraluminum baseplate by neoprene gaskets. The larger chamber encloses the magnet system which is mounted on the baseplate. The smaller oven chamber encloses the source and calibration ovens. Each chamber, including the buffer chamber, is pumped by one or more liquid-nitrogen trapped oil diffusion pumps. The pressure in the large chamber is less than 10^{-6} millimeters of mercury under operating conditions. To allow easy access to its contents, each chamber may be removed from the baseplate and from the rest of the apparatus.

Two two-stage vacuum interlocks are provided, one in each of the main and oven chambers. The oven chamber interlock is used for the insertion and removal of the "oven bar" upon which the source and calibration ovens are mounted. The main chamber interlock is used for insertion and removal of the "button bar" with which collecting surfaces are placed at the detector position in the machine. This latter facility is necessary because the activity deposited on the collecting surface must be removed from the machine to be counted.

3. The Magnet System

A perspective view of the magnet system is shown in Figure 4. The end of the oven bar can be seen at the right and the end of the button bar is visible on the left. The Armco iron pole tips of the A and B magnets are sections of circular cylinders and provide a large region of relatively uniform field gradient. The inset in the lower left corner shows a scale profile of the A magnet pole tips. The dotted rectangle illustrates the region in which the field gradient is nearly constant and down which the

FIGURE 4

A perspective view of the magnet system. The A, C and B magnets are designated 1, 2, and 3 respectively. Also shown is the button interlock (5), the stop wire mechanism (6), and a portion of the oven interlock (4). The inset shows a profile of the A magnet pole tips and the region through which the beam passes.

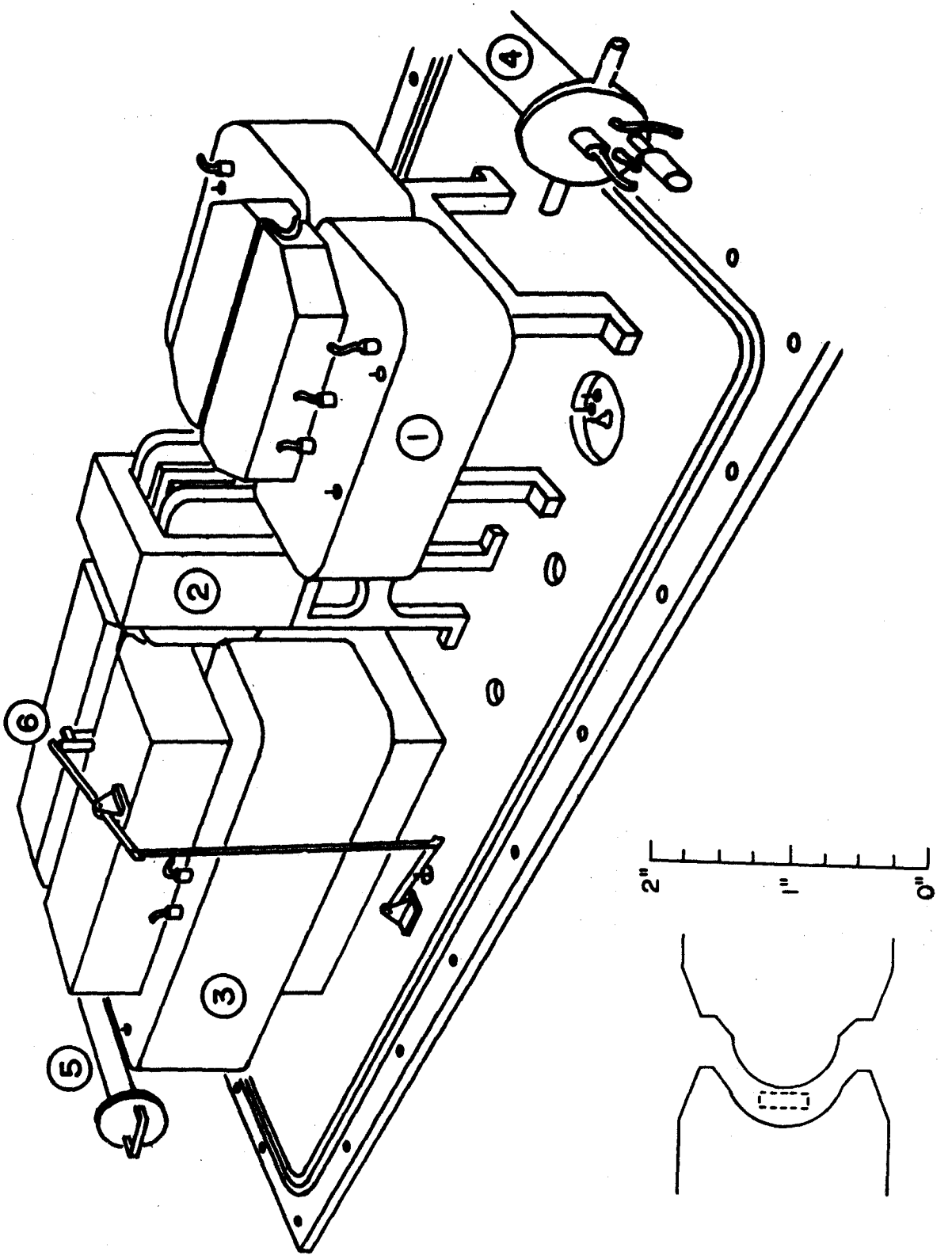
1
2
3
4
5
6
2"
1"
0"

beam travels. The B magnet shape is identical to that of the A magnet except that the linear dimensions of the B magnet are twice those of the A magnet in order to subtend approximately the same angle at the source.

Power for the high-impedance windings of the A and B magnets is supplied by a current regulated power supply capable of delivering 2 amperes at 2000 volts. For these experiments a magnet current of 1 ampere was used. The winding of the A magnet is tapped such that up to three-quarters of the A magnet coil may be shorted out. This provision is made so that the field of the A magnet may be varied in order that the focussing condition (equation (3-22)) may be optimized for the element being studied. For these experiments the fields in the A and B magnets were approximately 5 and 10 kilogauss respectively.

The C magnet has plane parallel pole tips and produces a uniform field. When these experiments were begun, the current for the C magnet coil was supplied by a voltage-stabilized power supply. Field instability proved intolerable, however, and the voltage stabilization was converted into current stabilization. After this modification, the C field was found to be stable to 1 part in 10^4 over a period of several hours. This fluctuation can be ascribed to changes in the fringing field of the A and B magnets rather than to the C magnet supply.

The C field is calibrated by observing the $(2,-2)\leftrightarrow(2,-1)$ transition in either sodium-23 or potassium-39. The known nuclear and electronic properties of these isotopes determine the $(2,-2)\leftrightarrow(2,-1)$ transition frequency, and a table has been calculated. Thus, one can obtain the field corresponding to any observed transition frequency. The observed resonance is broadened by inhomogeneities in the C field. This broad-

ening, about 200 kilocycles per second at 230 gauss, limits the accuracy to which the transition frequency may be obtained. Typically, the peak of the resonance is uncertain by about 10 or 15 kilocycles per second corresponding to a field uncertainty of about 0.02 gauss at 230 gauss.

4. Source and Calibration Ovens

For reasons discussed in the next chapter, the source ovens used for the silver experiments were heated to about 1450°C. in order to produce a silver beam. In order to reach this temperature, a smaller oven than described in the references at the beginning of this chapter was used. This is illustrated in Figure 5. The oven was constructed of tantalum. The 1/16-inch thick jaws of the adjustable slit were set to provide a slit 0.005 inches wide. Previous experience had shown that the recessed lid remained at the same temperature as the oven and thus prevents condensation of the source material on the bottom of the lid (Eastwood, 1964). The oven was heated by electron bombardment from two thoriated tungsten filaments strung vertically in front of the oven.

The calibration oven contained the calibration material, in this case either potassium or sodium, and was similar in design to the source oven. Since potassium and sodium beams can be produced at a temperature of about 500°C., the calibration oven was made of stainless steel and was directly heated by a tungsten filament.

All electrical leads for the heating of both ovens pass through a Kovar seal in the oven bar upon which the ovens are mounted.

5. Radiofrequency Equipment

The transition frequencies observed in these experiments ranged from 1 to 600 megacycles per second. The higher frequencies were required for

FIGURE 5

The source oven used for the silver-109m experiments. All parts of the oven are fabricated from tantalum.

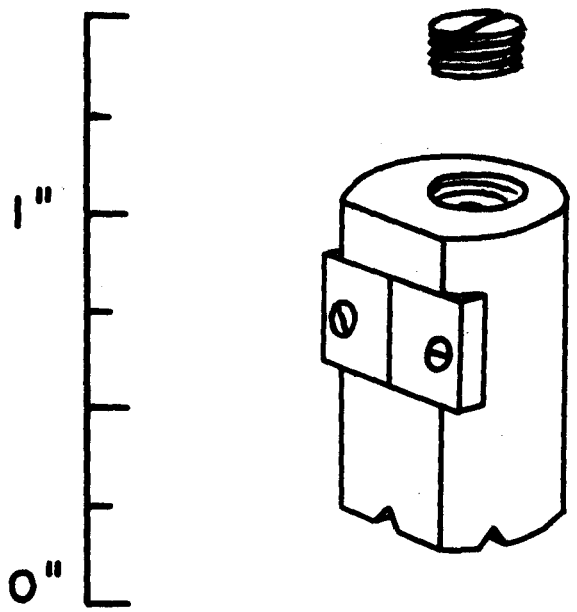
1"
0"

C magnet calibration. Listed in Table I are the radiofrequency oscillators used together with the manufacturer's specifications. The power amplifier is useful when high power is needed to induce multiple quantum transitions. As these experiments were nearing completion, a Weinschel Engineering Model DS109H double-stub tuner became available. The tuning stub was used to minimize the reflected wave from the r.f. loop.

The r.f. loop consisted of a U-shaped piece of 20 gauge copper wire terminating a section of coaxial line. The loop was mounted with its magnetic field parallel to the beam and normal to the C field. Sufficient power could be delivered to the loop to excite transitions involving up to four quanta.

A Beckman Model 7170 electronic counter and Series 7570 frequency converter were used to monitor the radiofrequencies. The counter is stabilized by an internal crystal-controlled 1 megacycle per second oscillator which has a short-term stability of 1 part in 10^7. Corrections for long term drift are made with periodic checks against the 5 and 10 megacycle per second standard transmissions of WWV. Overall accuracy in frequency measurements is 1 part in 10^6.

6. Beam Detection

Detection of the alkali calibration beam and of the radioactive source beam is carried out by two different methods. The radioactive beam is collected on a surface which is then removed from the machine for counting. The alkali beam is detected with a surface ionization detector.

The latter works on the principle that a fraction of the atoms evaporating from a hot surface are emitted as ions if the ionization potential of the atoms is lower, or not much larger, than the work function of the surface. The hot surface is provided by a pure tungsten wire (whose

TABLE I

Radiofrequency Equipment

Manufacturer	Model	Frequency Range (Mc/Sec)	Power Output (Watts)
Tetronix	190A	0.35 - 50	2 into 50 ohms
Wandel and Goltermann	LMS-68	with the following plug in units	
	LO-4	4 - 40	1 into 60 ohms
	LO-40	40 - 108	1 into 60 ohms
	LMS-681	75 - 160	1 into 60 ohms
	LO-170	170 - 330	1 into 60 ohms
	LO-325	325 - 610	0.5 into 60 ohms
	LO-610	610 - 960	0.5 into 60 ohms
Boonton Radio Corporation	230A	10 - 500	4 into 50 ohms

surface may be oxidized by residual oxygen in the vacuum system), 0.008 inches in diameter and about two inches long, heated to about 1600°C. by a current of 4 amperes. The wire is mounted vertically so as to intercept the atoms leaving the B magnet exit slit and is kept at a positive potential to drive the ions away. The ion current is collected on a nichrome strip and measured with a Victoreen model VTE-2 electrometer. On resonance, an ion current of about 10^{-11} amperes is obtained. The background noise of the detector is less than 10^{-12} amperes.

The radioactive beam is collected on a standard surface, or "button", for a fixed length of time. The button is then removed from the machine and placed in a counter where the decay of the activity on the surface is followed. Preliminary experiments are made to determine what type of surface is most efficient as a collector.

In this laboratory, thin-window β-counters are used to count the activity on the button surfaces. These consist of Philips' type 18515 end-window geiger tubes together with their surrounding type 18517 guard tubes. The outputs are fed into a transistorized anti-coincidence unit and the counts are displayed by a R.E.A.C. model E-110 scaler. A background counting rate of about 2 counts per minute is obtained when the counting tubes are enclosed in a castle made from 2-inch thick lead bricks.

7. General Experimental Procedure

Prior to an experiment, one must decide what frequency range will be examined and the number of exposures that will be made over this range. The latter is limited by the length of time that the beam will last, whereas the frequency range to be scanned is dictated by the uncertainty in the anticipated position of the resonance.

Having made these decisions, one sets the C field at the desired value. The field is left to stabilize for a few hours and checked again. The experiment is then begun. Resonance exposures are made at frequencies scattered randomly through the search range in order to minimize the effect of field drift. Beam intensity is monitored throughout the experiment by exposing buttons with the "stop-wire" removed. These buttons, referred to as "half beam" exposures, sample those beam atoms which are undeflected by the A and B magnets by virtue of their high velocity or zero effective moment. In this manner, variations in beam intensity may be noted and the results from the resonance exposures corrected for any such variations. Several buttons are exposed with the "stop-wire" in but with the r.f. turned off. These exposures give a measure of machine background. The C field is checked at least every two hours and at the end of the experiment.

The counting rate is determined for each button, and the half-beam counting rates are plotted as a function of time. This allows interpolation of the beam intensity at the time of any given resonance exposure. The exposure counting rates are then normalized to constant beam intensity by means of this curve. A resonance curve is obtained by plotting these normalized counting rates, together with their statistical uncertainties, against their corresponding frequencies.

In the silver experiments, it was found that multiple quantum transitions were being observed. Since the intensity of such transitions is very dependent on r.f. power, the r.f. power was maintained as constant as possible on any given day. The double-stub tuner was used to obtain the minimum V.S.W.R. over the frequency range being swept.

CHAPTER V

THE SILVER EXPERIMENTS

1. Source and Beam Production

The silver-109m ($T_{1/2}$ = 41 seconds) studied in this experiment was produced by the decay of palladium-109 ($T_{1/2}$=13.5 hours). The radioactive palladium was obtained from the $Pd^{108}(n,\gamma)Pd^{109}$ reaction by neutron bombardment of natural palladium in the McMaster nuclear reactor. Palladium-108 has an isotopic abundance of 26.71% and a thermal neutron cross-section of 12 barns for the production of 13.5 hour palladium-109. Prior to irradiation, the palladium was ground to a fine powder and then sealed in a quartz capsule. A specific activity of 3 millicuries per milligram of palladium was obtained following a twelve-hour irradiation in a flux of 2×10^{13} neutrons/cm^2/sec. A 20 milligram source was used for the spin searches but the source size was increased to 50 milligrams for the magnetic moment investigations.

The active palladium was allowed to sit for six or seven hours after irradiation in order to allow any palladium-111 which was produced to decay. The neck of the quartz tube was then broken and the palladium mixed with an equal volume of finely ground carbon. This mixture, along with some samarium and sodium, was placed in the source oven. The latter was mounted on the oven bar, and inserted into the machine.

The oven was then gradually heated to operating temperature. A sodium beam was produced first and was used for alignment of the source oven. This beam also provided another field calibration. As the oven temperature increased, a samarium beam was produced. This was used for

final alignment of the source oven. At this point, a telescope was focussed on the oven and the cross-hairs were adjusted to coincide with the edge of the oven. These steps were necessary because silver cannot be detected with the surface ionization detector . Since the source oven had to be moved to allow C-field calibration during the experiment, the telescope setting could be used to reposition the source oven following calibration. The oven was then brought to an operating temperature of about 1450°C. At this temperature, the vapour pressure of palladium is about 7×10^{-3} millimeters of mercury (Honig, 1962), and all sodium and samarium has been evaporated from the oven. The experiment was begun about twenty mimutes later. This time delay was necessary to allow the oven surroundings in the oven chamber to outgas.

At operating temperature, the active silver diffused out of the palladium and formed a steady carrier-free silver beam. An abrupt decrease in beam intensity occurred in the first experiments about one hour after the experiment was begun. This is believed to have been caused by the palladium sintering after prolonged heating at this high temperature. Because of this, in later experiments, the active palladium was mixed with the ground carbon. This prevented sintering and a steady beam of silver could then be produced. Since the silver beam is produced from a parent with a 13.5 hour half-life, a useful silver beam could be produced from the palladium for a time comparable to this.

2. Beam Detection

Preliminary experiments were necessary to determine what type of surface would collect the silver beam most efficiently. Copper, silver, antimony, sulphur, and steel surfaces were tested and it was found that copper and steel surfaces had the best collection efficiencies. Being

easiest to prepare, steel collection surfaces were used in subsequent experiments.

In order to count the silver-109m, it was necessary to detect the conversion electrons from the 88-keV ground state transition. Experiments were conducted to determine whether solid-state surface-barrier detectors or conventional thin-window Geiger tubes should be used as detectors. A Ni^{63} source (β-end point energy = 63 keV) was used in these experiments. An ORTEC surface-barrier detector with 25 mm^2. active area was compared with a Philips' 18515 Geiger tube. The small area of the surface-barrier detector was necessitated because low detector noise was required. A 50 mm^2. detector was also tested but proved much noisier than the smaller detector. Although the signal-to-noise ratio of both detectors was about the same, the absolute counting rate of the Geiger counter was a factor of about twenty higher than that of the surface-barrier detector. An x-ray crystal was also tested using half-beam buttons as sources. Again the Geiger counter proved a much superior detector. As a result of these findings, the Geiger counter was used in all subsequent experiments.

3. The Spin Search for Silver-109m

Using the known g_J-value of silver*, the frequencies of the Zeeman transitions were calculated from equation (3-17) for half-integral values of nuclear spin from I = 1/2 to I = 13/2. The result of a spin search at 7.04 gauss is shown in Figure 6. In this figure (and all subsequent figures

---

* The ratio g_J (Ag) / g_J(K) has been determined by S. Penselin (private communication, 1964) to be 1.000026(2) and a recent measurement at Berkeley (private communication from H. A. Shugart, 1966) yields $g_J(K) = -2.0022954(22)$. Thus $g_J(Ag) = -2.0023475(50)$.

FIGURE 6

The results of a silver-109m spin search at 7.04 gauss. The open circle and dashed line indicate machine background.

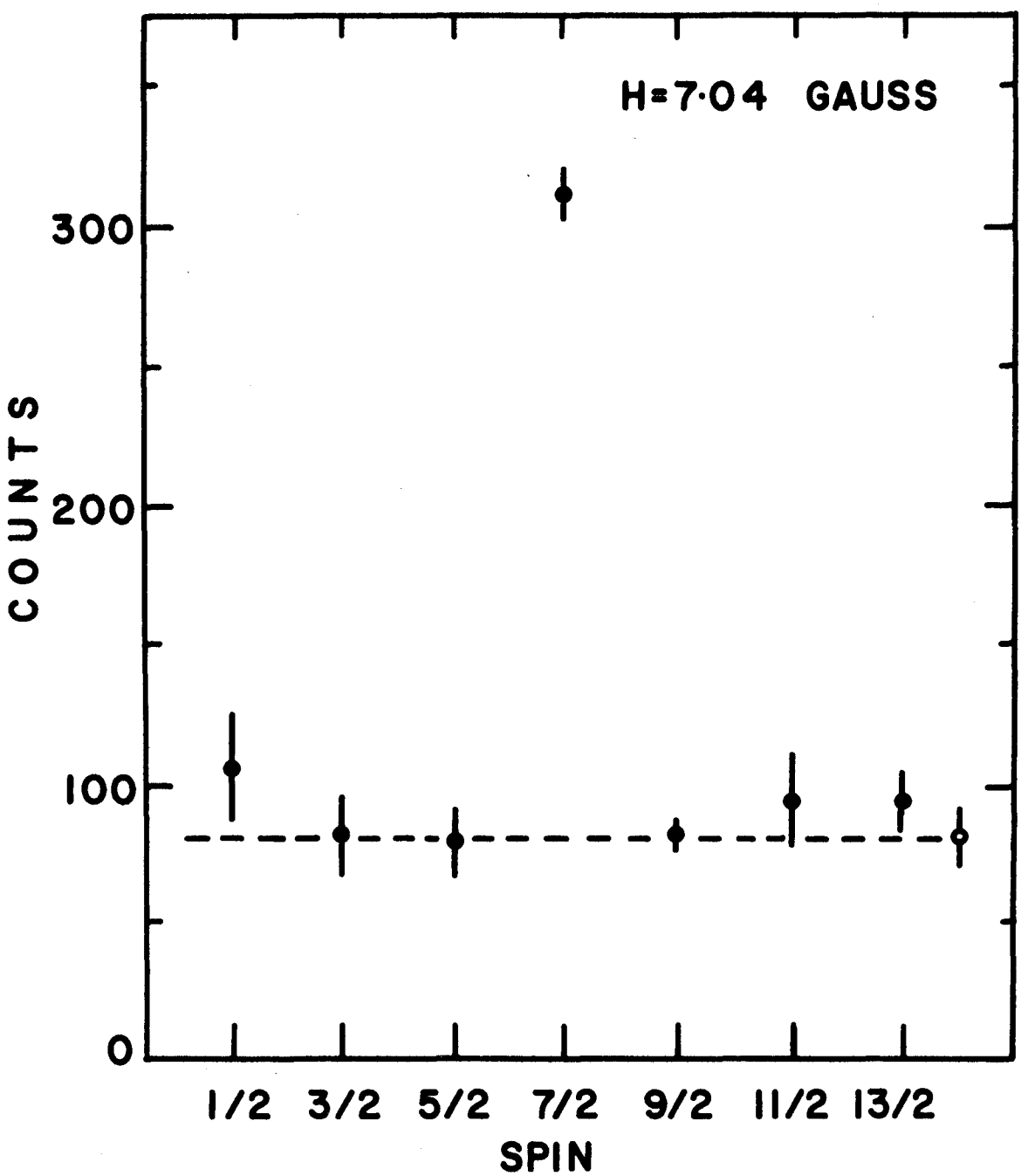
H=7·04 GAUSS
300
200
100
0
COUNTS
1/2
3/2
5/2
7/2
9/2
11/2
13/2
SPIN

displaying experimental results), the open circle and the dashed line represent machine background. From this figure, it is apparent that a spin-7/2 activity is present. To assure that the detected activity was silver-109m, the decays of several monitor and resonance exposures were followed. Typical resonance and monitor exposure decays are shown in Figure 7; the lines are drawn to correspond to a 41-second half-life.

A detailed study of the resonance shape was made at 5.77 gauss and the results are shown in Figure 8. In this diagram, ν_{Nom} is defined as

$$\nu_{Nom} = \frac{-g_J \mu_o H}{(2I+1)\ h} \qquad (3\text{-}17)$$

and is calculated for I = 7/2.

From the results of these experiments, it is concluded that the nuclear spin of silver-109m is I = 7/2.

4. The Magnetic Moment Determination for Silver-109m

As indicated in Chapter III, the magnetic field must be increased in order that the effect of a finite hyperfine splitting may be seen. The resonance shape obtained at 100.04 gauss is shown in Figure 9. Comparing this figure with Figure 8, one immediately notices that the high field resonance has become double and that each of these peaks is much wider than the low-field resonance.

In Chapter III, it was suggested that a large hyperfine splitting could be expected in silver-109m, and, this being the case, unusual transitions could be focussed. Proceeding on this assumption, and taking $\mu_I > 0$, the frequencies were calculated at which multiple quantum transitions from the (F=4,M=-4), (F=4, M=-3), and (F=3, M=-3) levels would occur. These are plotted in the upper portion of Figure 9 for nuclear moments from 3.5 to 5.5 nuclear magnetons. The range is limited here solely for

FIGURE 7

Typical decay curves for the activity deposited on the collector buttons. The open and solid circles are for a monitor and resonance exposure respectively. The lines are drawn to correspond to a 41-second half-life.

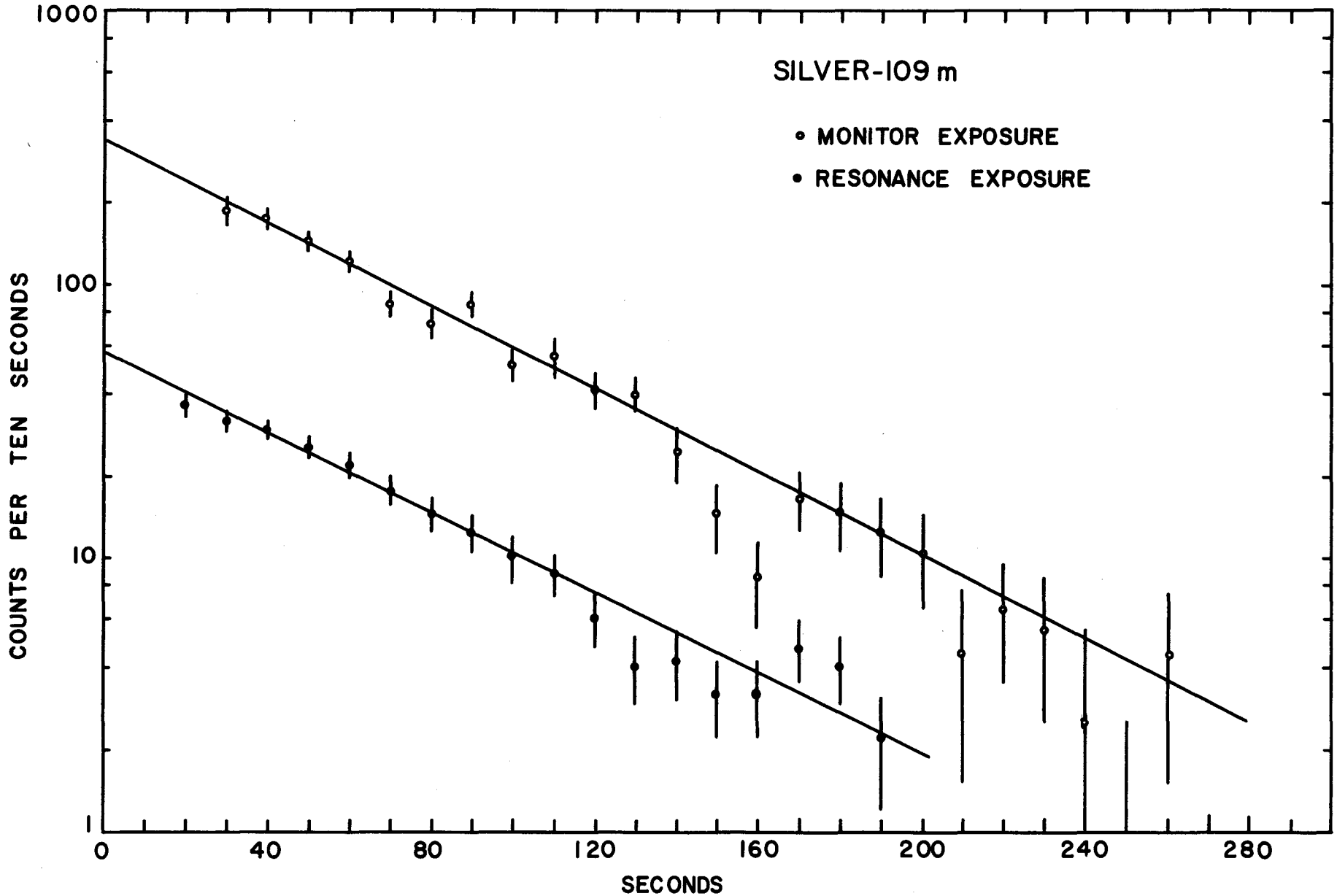
SILVER-109 m
MONITOR EXPOSURE
RESONANCE EXPOSURE
COUNTS PER TEN SECONDS
1000
100
10
1
0
40
80
120
160
200
240
280
SECONDS

FIGURE 8

A resonance curve in silver-109m obtained at a field of 5.77 gauss. The arrow indicates the expected position of a spin -7/2 resonance at this field.

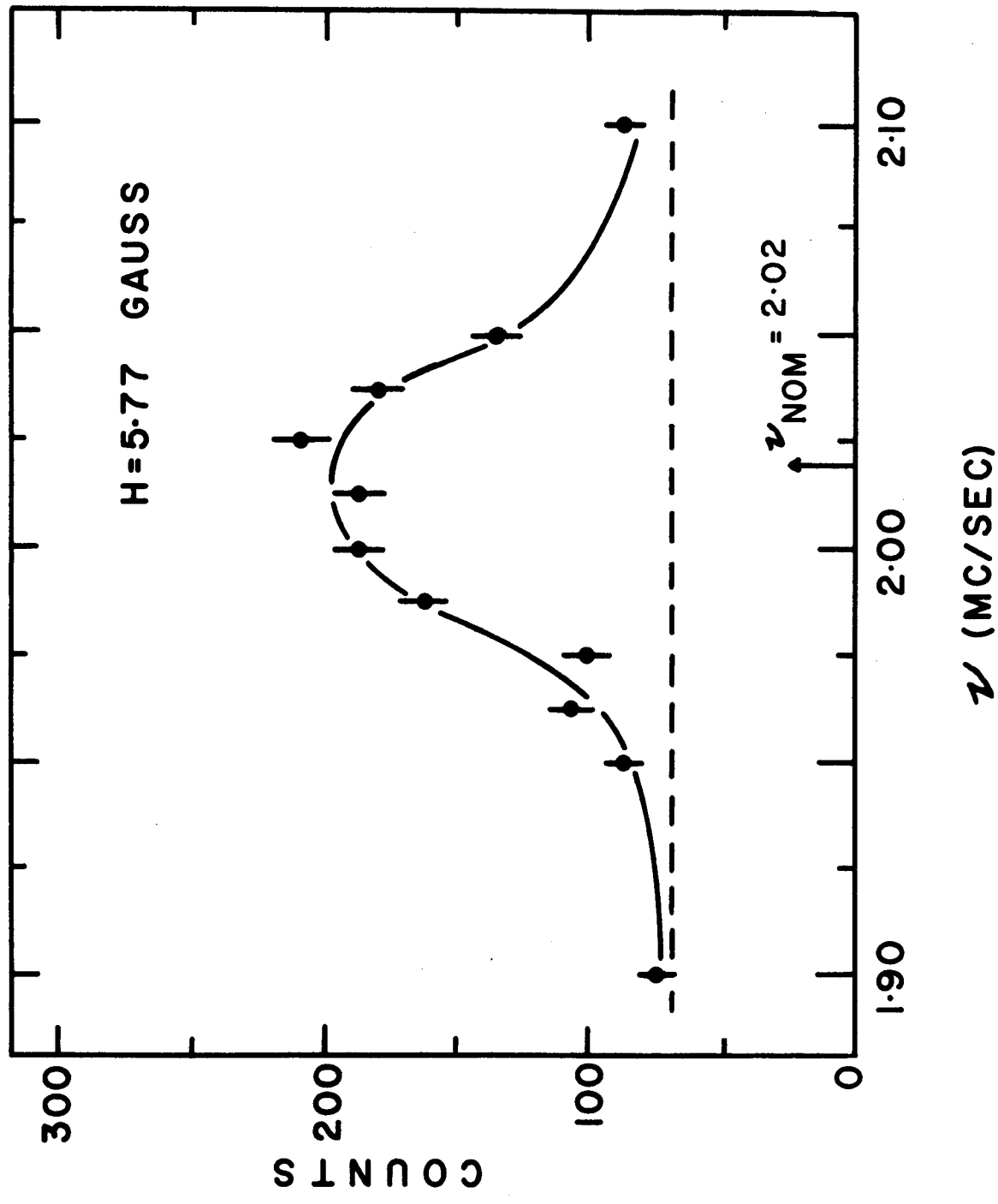
H=5·77 GAUSS
COUNTS
300
200
100
0
1·90
2·00
2·10
ν_{NOM} = 2·02
ν (MC/SEC)

FIGURE 9

The resonance curve in silver-109m obtained at a field of 100.04 gauss. The arrow indicates the expected position of a spin-7/2 resonance at this field assuming a large hyperfine separation and negligible nuclear moment. In the upper portion of the figure, the frequencies at which multiple quantum transitions in the upper and lower hyperfine multiplets would occur are plotted over a limited range as a function of nuclear moment. The F-values are interchanged for $\mu_I < 0$.

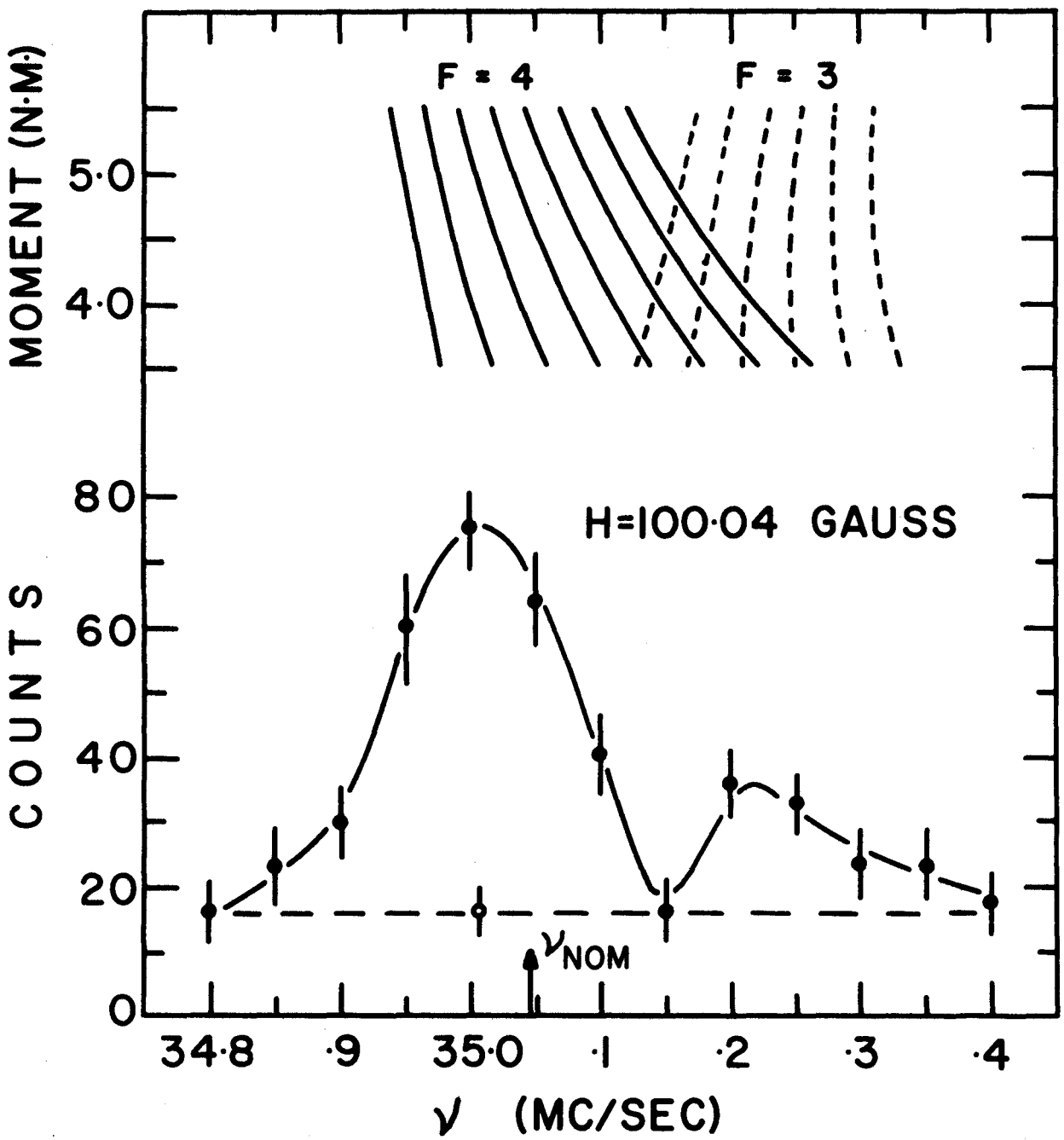
F = 4
F = 3
MOMENT (N·M)
5·0
4·0
COUNTS
80
60
40
20
0
H=100·04 GAUSS
ν_{NOM}
34·8
·9
35·0
·1
·2
·3
·4
ν (MC/SEC)

convenience; in fact, all possible values were considered. For negative moments, one must change the sign of M. The positions of the F=4 and F=3 transitions become interchanged on the graph. At this field, except for moments whose absolute values are less than about 1 nuclear magneton, n' transitions occur at the same frequency as the (n+2) transitions.

On this basis, the double resonance at 100.04 gauss can readily be explained. The low-frequency peak is due to multiple quantum transitions in the F=4 multiplet, and the high-frequency peak arises from multiple quantum transitions in the F=3 multiplet if the nuclear moment is positive and vice-versa if the nuclear moment is negative.

That the relative heights of the two peaks is not the same can also be justified on this interpretation. As was explained in Chapter III, since the deflecting magnets run at different fields, most of the transitions are expected to occur in one direction only; that is, transitions <u>from</u> the F=3, M=$\mp$3 level (the upper sign for $\mu_I > 0$, the lower for $\mu_I < 0$) will be focussed but transitions <u>to</u> this level will not be and similarly for the others. Because one pole tip of the deflecting magnet is convex and the other concave, transmission through the magnet would be greater for atoms deflected towards low field. It is not obvious that the A and B magnet pole gaps play equivalent roles in limiting the beam transmission. Thus, although the n' and n'' transitions are mirror images of each other as far as the energy diagram is concerned, they need not contribute equally to the detected beam. Also occurring in the F=4 multiplet are the n transitions. These contribute to the low-frequency peak if $\mu_I > 0$ and to the high-frequency peak if $\mu_I < 0$. The fact that the low-frequency peak was found to be the larger is suggestive that $\mu_I > 0$, but, in view of the

argument just given, this may not be taken as proof of the sign of the moment.

The field was now increased in order to separate the multiple quantum transitions. Figure 10 is a composite of the results of several runs at 230 gauss. There are now five distinct resonances in the frequency range scanned. A diagram of the calculated frequencies of the n ,n', and n'' transitions for nuclear moments from -6.5 to +6.5 nuclear magnetons is shown in Figure 11. Still, the n' transitions occur at essentially the same frequencies as the (n+2) transitions.

The four low-frequency peaks were obtained first. From Figure 11, it can be seen that these four resonances would be explained if the nuclear moment were either about 4.5 or about 5.5 nuclear magnetons. No other value of nuclear moment, either positive or negative, can explain the positions of all four of these resonances.

In order to decide which of the two values for the moment was correct, a transition was sought that would rule out one of these two values. The resonance at about 81.5 megacycles per second was obtained. The presence of such a resonance is consistent with a nuclear moment in the range from 4.1 to 4.7 nuclear magnetons or greater than about 6.5 nuclear magnetons. There is no transition by which this resonance can be explained for a nuclear moment of about 5.5 nuclear magnetons.

From the results at 230 gauss, it is concluded that the nuclear moment of silver-109m is about +4.5 nuclear magnetons. The transitions that have been observed are interpreted as being, in order of increasing frequency, a 6 or 4' transition, a 5 or 3' transition, a 4 or 2' transition, a 4'' transition, and a 2'' transition. No attempt was made to find the 3''

FIGURE 10

A composite plot of the results obtained in silver-109m at a field of 230 gauss. For reasons discussed in the text, part of the frequency region shown was not investigated.

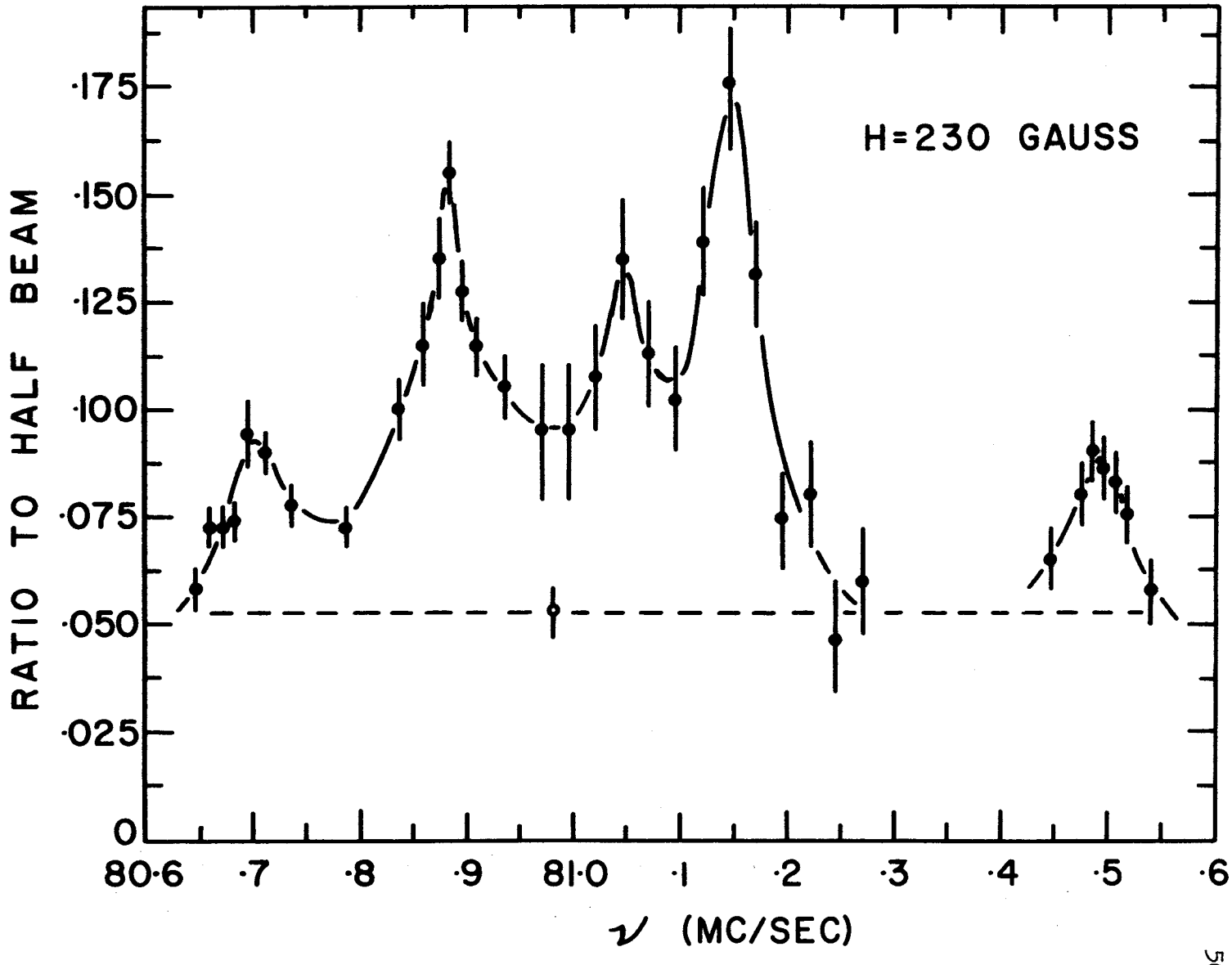
H=230 GAUSS
RATIO TO HALF BEAM
·175
·150
·125
·100
·075
·050
·025
0
80·6
·7
·8
·9
81·0
·1
·2
·3
·4
·5
·6
ν (MC/SEC)

FIGURE 11

Calculated frequencies of various multiple quantum frequencies as a function of moment at a field of 230 gauss. Unless shown otherwise, n^{1} and (n+2) transitions occur at essentially the same frequency at this field. The solid rectangles between the horizontal lines at a moment of about 4.5 n.m. indicate the frequencies of the observed resonances at 230 Gauss.

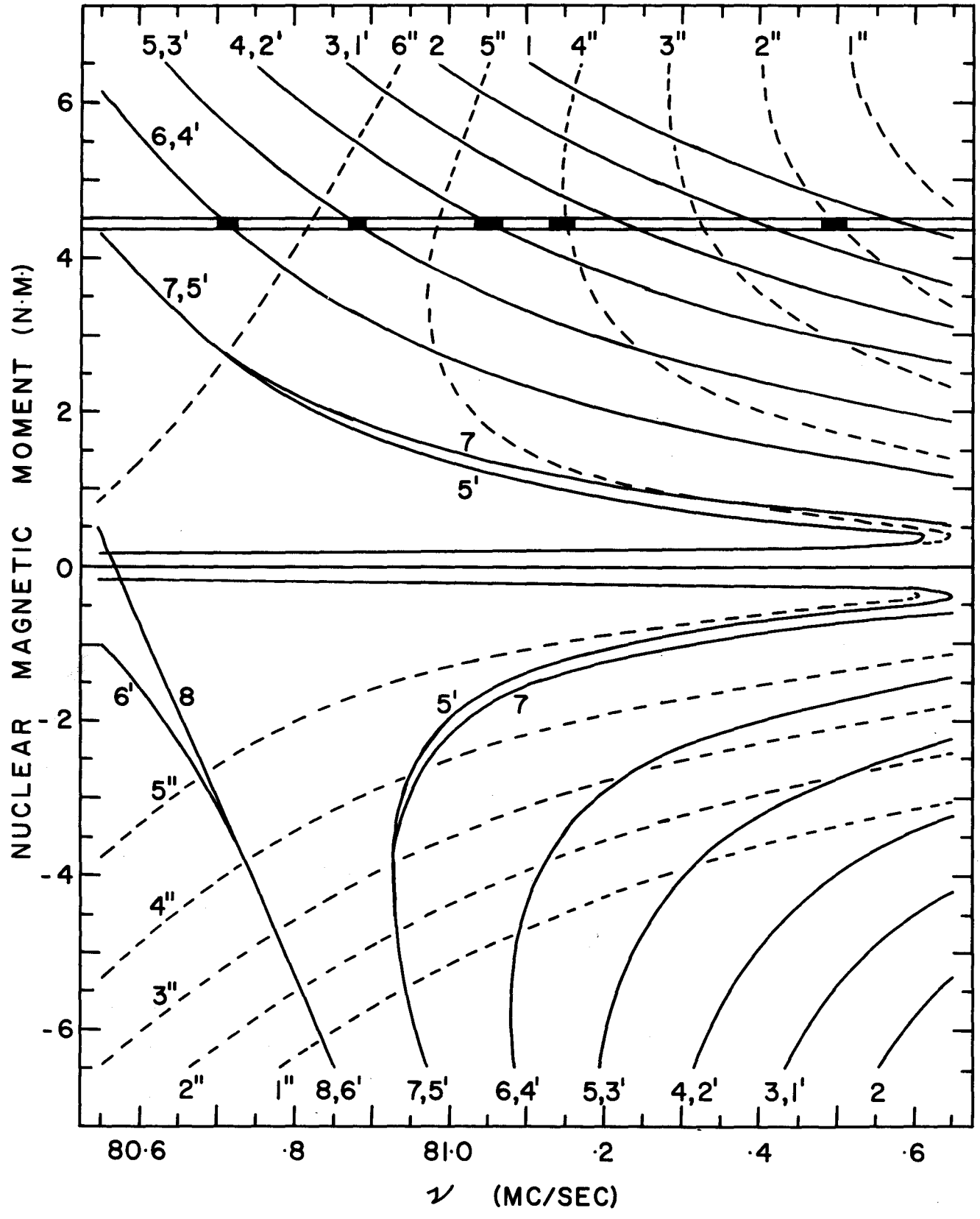
5,3'
4,2'
3,1'
6"
2
5"
1
4"
3"
2"
1"
6,4'
7,5'
7
5'
6'
8
5'
7
5"
4"
3"
2"
1"
8,6'
7,5'
6,4'
5,3'
4,2'
3,1'
2
6
4
2
0
-2
-4
-6
NUCLEAR MAGNETIC MOMENT (N·M)
80·6
·8
81·0
·2
·4
·6
ν (MC/SEC)

transition. This interpretation is supported somewhat by the weaker features of Figure 10. The high-frequency tail of the resonance at 81.150 megacycles per second may be due to a weak 3 or 1' transition, whereas the relatively high "valley" at about 81.0 megacycles per second may be caused by a weak 5" transition. Similarly, a weak 6" transition may be contributing to the low-frequency tail of the transition at 80.885 megacycles per second.

The field was increased to about 340 gauss in order to obtain a more precise value of the magnetic moment. The resonances found are shown in Figure 12, and Figure 13 is a plot of the frequencies at which the multiple-quantum transitions occur at 338.815 gauss. At this field, the observed transitions, in order of increasing frequency, are interpreted as a 6 or 4' transition, a 5 or 3' transition, a 4" transition, a 4 or 2' transition, a 3" transition, and a 2 transition. The curves of Figure 13 labelled n,(n-2)' are actually the averages of the n and (n-2)' transition frequencies since, even at 340 gauss, these transitions are separated by only 10 kilocycles per second. Not all of the possible transitions were searched for at 340 gauss, since additional transitions would add little to the accuracy of the result.

In order to separate the n and (n-2)' transitions by 100 kilocycles per second, a magnetic field of about 800 gauss would be required. At this field strength, two experimental difficulties were anticipated. First, it was suspected that the magnet supplies did not have the stability required. A stability of at least 0.02 gauss is essential over a period of about an hour in order to get meaningful results. Second, it was doubted whether the transitions would be intense enough. This suspicion is based upon the decrease in intensity of the resonances as the field was in-

FIGURE 12

Resonances observed in silver-109m at a field of about 340 gauss. In order of increasing frequency, the transitions were identified as a 6 or $4'$ transition, a 5 or $3'$ transition, a $4''$, a 4 or $2'$ transition, a $3''$ transition, and a 2 transition.

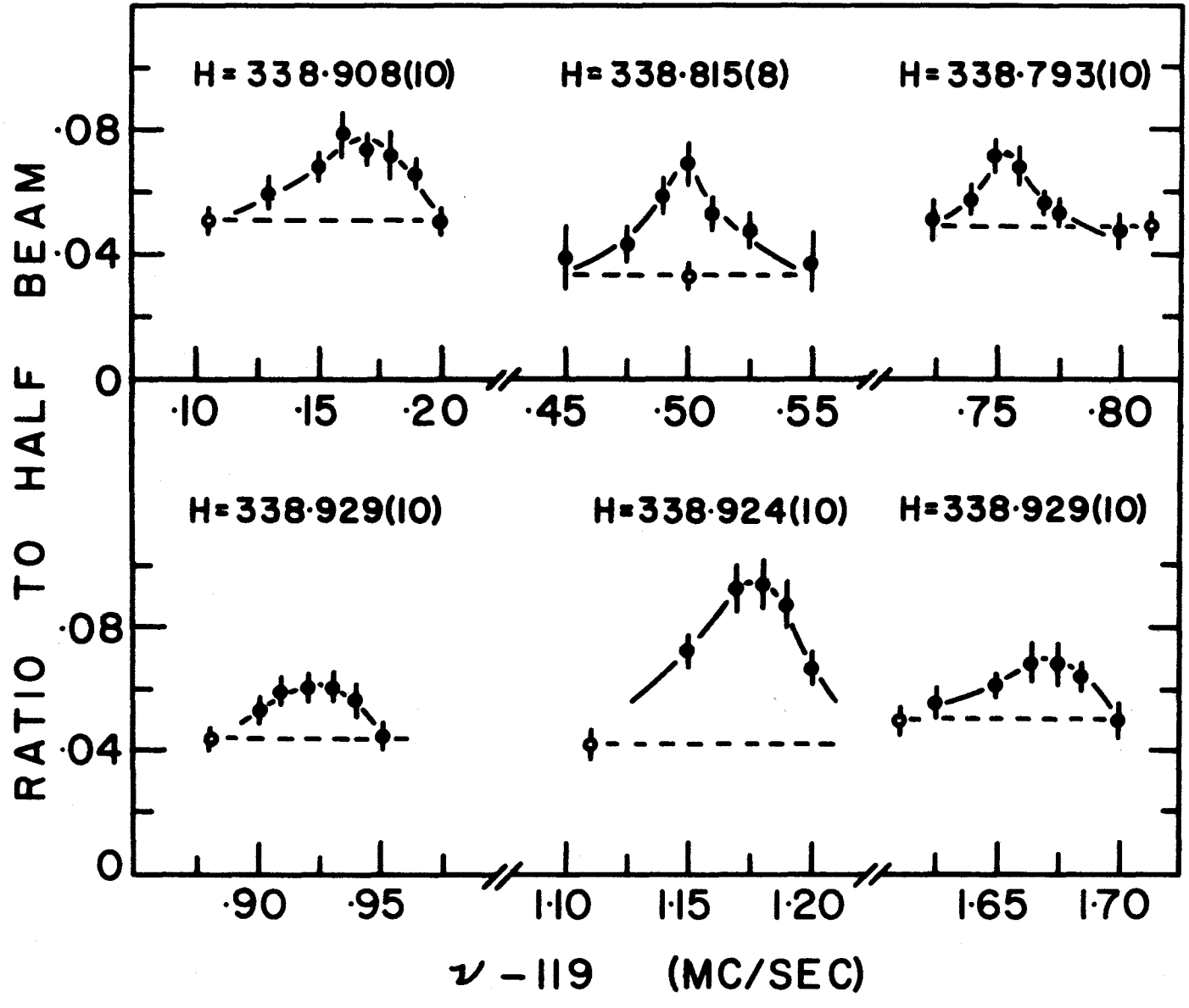
H = 338·908(10)
H = 338·815(8)
H = 338·793(10)
H = 338·929(10)
H = 338·924(10)
H = 338·929(10)
RATIO TO HALF BEAM
·08
·04
0
·10
·15
·20
·45
·50
·55
·75
·80
·90
·95
1·10
1·15
1·20
1·65
1·70
ν − 119 (MC/SEC)

FIGURE 13

Calculated frequencies of the various multiple quantum transitions as a function of magnetic moment at a field of 339 gauss. The solid blocks indicate the positions of observed resonances.

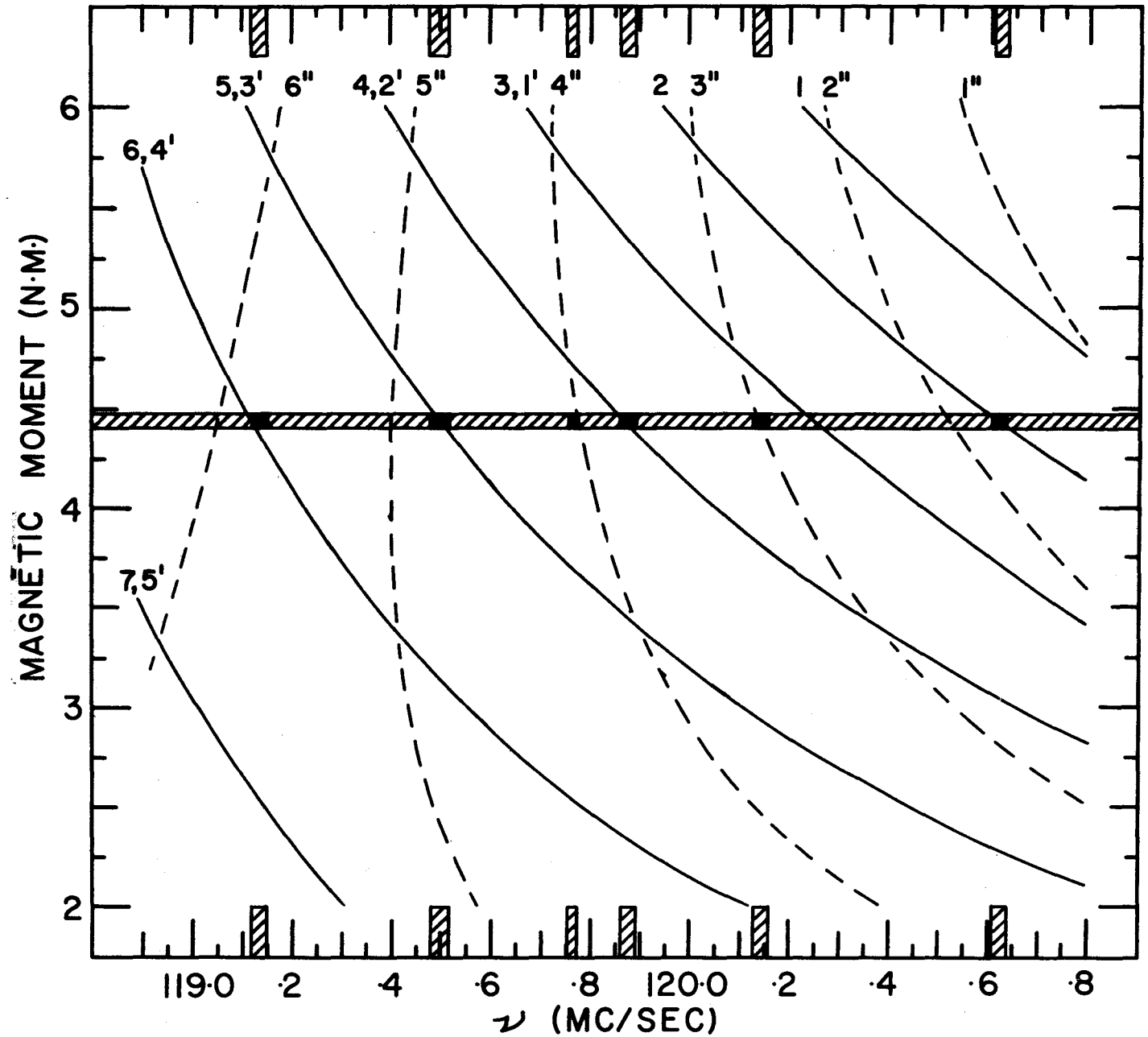
6,4'
5,3' 6"
4,2' 5"
3,1' 4"
2 3"
1 2"
1"
7,5'
MAGNETIC MOMENT (N·M)
6
5
4
3
2
119·0
·2
·4
·6
·8
120·0
·2
·4
·6
·8
ν (MC/SEC)

creased from 230 to 340 gauss. It was decided to attempt experiments at the intermediate field of 500 gauss in order to see if experiments at 800 gauss would be feasible.

Preliminary experiments with sodium showed that the field was indeed unstable even at 500 gauss. Sudden field shifts, together with oscillations about a mean value were noted. Many attempts were made to obtain silver-109m resonances. Figure 14 shows the resonances obtained. The extreme intensity and narrowness of these resonances are immediately apparent. In order of increasing frequency, these transitions were identified as a $3'$ transition, a 5 transition, a $2'$ transition, and a 4 transition.

The first of these resonances was obtained while sweeping, in 5 kilocycle per second steps, the region where the $2'$ resonance was expected. One extremely high point, which remained high on another exposure, was found. The field was immediately calibrated, and the region of the high point was swept in one kilocycle per second steps. After several field shifts, the field remained stable enough to plot out a resonance shape. The field was then recalibrated. The procedure from calibration to calibration took about forty minutes. The identity of this transition was not known, but calculation showed that the "partner" resonance would be about 25 kilocycles per second either above or below the observed transition frequency depending on whether a $2'$ or a 4 transition had been observed. Since another less intense resonance (the curve shown in the lower right of Figure 14) was obtained at the higher frequency alternative, the identity of these transitions was established. The frequencies of the $3'$ and 5 transitions could then be calculated, and, after several more searches, the resonance corresponding to these transitions were obtained. These resonances are shown at the top of Figure 14.

FIGURE 14

The resonances obtained in silver-109m at a field of about 500 gauss. In order of increasing frequency, these transitions were identified as a $3'$ transition, a 5 transition, a $2'$ transition, and a 4 transition.

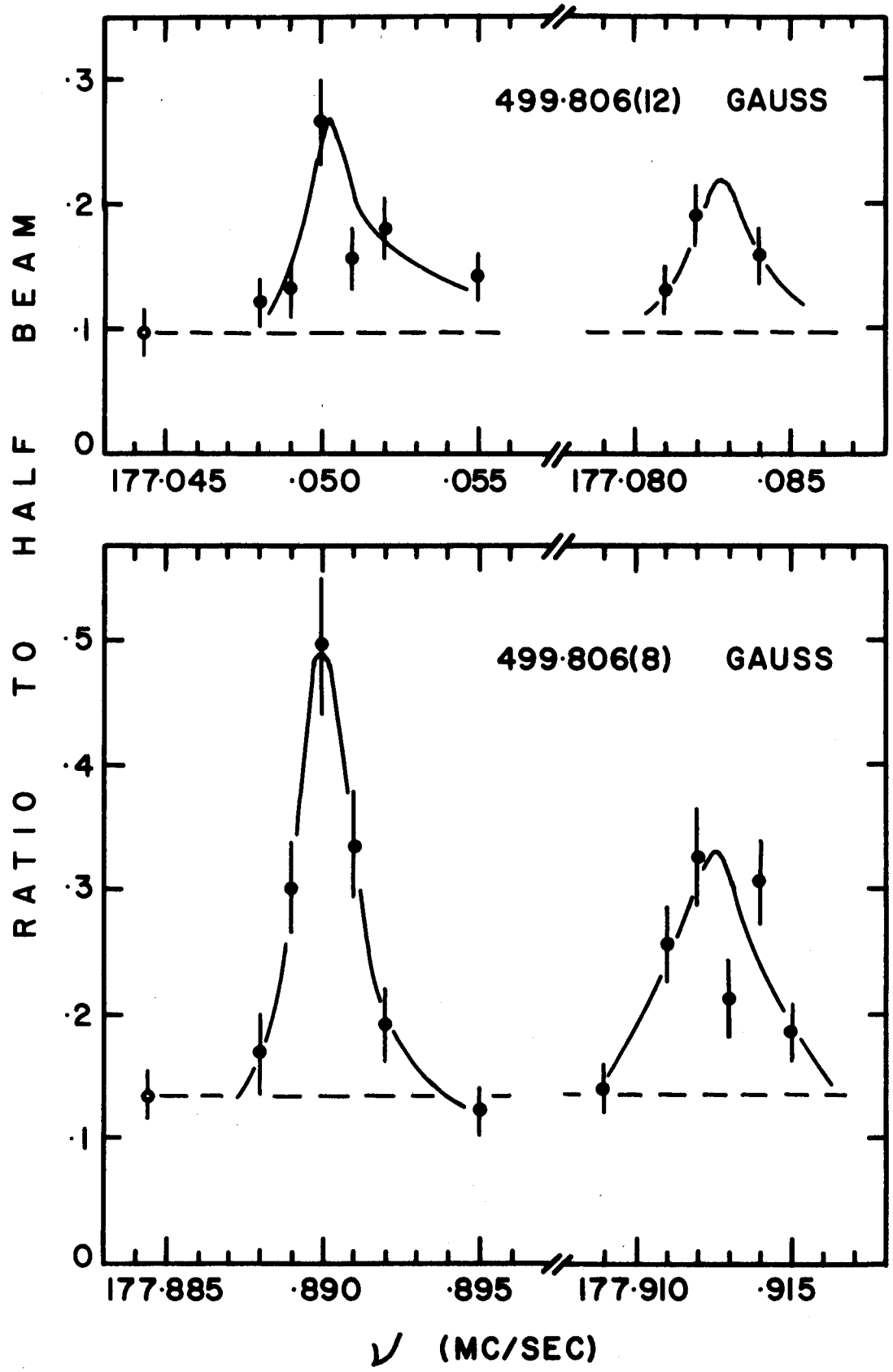
499·806(12) GAUSS
499·806(8) GAUSS
RATIO TO HALF BEAM
·3
·2
·1
0
·5
·4
177·045
·050
·055
177·080
·085
177·885
·890
·895
177·910
·915
ν (MC/SEC)

A search for corresponding n' and n'' transitions was begun in order to obtain a direct measurement of μ_I following the method suggested by equation (3-28). Although a considerable amount of time was spent looking for these n'-n'' resonance pairs, field instability proved intolerable and none of them were observed. It was decided at this point to discontinue these experiments until a more stable field was available.

A two-parameter non-linear least squares program was written for the IBM-7040 computer at McMaster, and was used to fit the experimental data. The data were best fit if it was assumed, whenever there was a choice, that n' transitions rather than (n+2) transitions had been observed. This interpretation is supported by the resonance shape observed at 500 gauss where the n' transitions are more intense than their (n+2) partners. The best-fit values for the atomic and nuclear parameters, as determined by this computer routine, are

$$g_I = +(6.71 \pm 0.06) \times 10^{-4} \quad \text{giving} \quad \mu_I(\text{uncorrected}) = 4.31 \pm .04 \text{ n.m.}$$

and $$\Delta\nu = 37908 \pm 49 \text{ Mc/sec} \quad \text{giving} \quad a = 9477 \pm 13 \text{ Mc/sec.}$$

A tabulation of the observed transition frequencies, together with those predicted using the best-fit values given above, is presented in Table II. For these calculations, the g_J-value of silver that was used was $g_J(Ag) = -2.002350$ (see footnote on page 48). An independent fit* to the data with the "Hyperfine-4" program used by the atomic beam group at Berkeley gives essentially identical values.

---

* This was carried out by Dr. Summers-Gill who was kindly allowed computer time on the IBM-7094 at Berkeley for this purpose. The assistance of members of the atomic beam group at Berkeley in providing a check of the author's computer results is greatly appreciated.

TABLE II

High Field Zeeman Transitions in Silver-109m

Initial F	Initial M	Final F	Final M	Field (Gauss)	$\nu_{Observed}$ (Mc/Sec)	$\nu_{Calculated}$ (Mc/Sec)	$\nu_{Obs}-\nu_{Cal.}$ (Mc/Sec)	Exp.Error* (Mc/Sec)
4	-4	4	0	499.806	177.913	177.913	0.000	0.003
4	-3	4	-1	499.806	177.890	177.889	0.001	0.003
4	-4	4	1	499.806	177.083	177.082	0.001	0.004
4	-3	4	0	499.806	177.050	177.050	0.000	0.004
4	-3	4	-1	338.929	119.923	119.933	-0.010	0.012
4	-3	4	-1	338.908	119.913	119.925	-0.012	0.013
4	-3	4	-1	338.900	119.910	119.923	-0.013	0.015
4	-3	4	0	339.031	119.571	119.588	-0.017	0.015
4	-3	4	0	338.815	119.500	119.511	-0.011	0.015
4	-3	4	1	338.908	119.167	119.168	-0.001	0.010
4	-3	4	1	338.815	119.141	119.135	0.006	0.025
4	-3	4	-1	229.948	81.035	81.047	-0.012	0.020
4	-3	4	-1	229.948	81.030	81.047	-0.017	0.015
4	-3	4	0	229.963	80.870	80.878	-0.008	0.020
4	-3	4	0	230.010	80.870	80.895	-0.025	0.025
4	-3	4	0	229.910	80.850	80.860	-0.010	0.010
4	-3	4	1	230.043	80.725	80.734	-0.009	0.015
4	-3	4	1	230.049	80.715	80.736	-0.021	0.015
4	-3	4	1	230.010	80.710	80.722	-0.012	0.025
3	-3	3	0	338.925	120.175	120.187	-0.012	0.015
3	-3	3	1	338.793	119.755	119.763	-0.008	0.010
3	-3	3	-1	230.014	81.500	81.503	-0.003	0.015
3	-3	3	-1	230.014	81.495	81.503	-0.008	0.015
3	-3	3	1	229.947	81.130	81.132	-0.002	0.015

* This error incorporates uncertainties in field calibration and in silver resonance position.

The chisquare for this fit is 12.5 which implies, for 24 points and only two parameters, a 95% probability that a random sample of data would give no better fit. These results predict a hyperfine anomaly between silver-109 and silver-109m of $-(1.1\pm1.2)$ percent. The data were also fitted assuming no hyperfine anomaly. This yielded a chisquare of 13.3. Thus, from the present results, the existence of a hyperfine structure anomaly cannot be established unequivocably.

For the computer fit, a $2'$ resonance observed at 499.795(12) gauss and a 2 resonance observed at 338.925(10) gauss were omitted. These transitions were predicted to occur at frequencies differing from the observed frequencies by about three times the quoted errors of the observations. The $2'$ resonance disagreed with the four resonances shown in Figure 14. This disagreement is most probably due to a field shift during the time the resonance profile was being obtained. Field shift is also the most likely cause of the discrepency of the 2 resonance position. This resonance is presently being re-investigated. In any case, even when these points are included, the best-fit values of g_I and $\Delta\nu$ lie just within the errors quoted above.

Most transitions at 230 gauss and 340 gauss are predicted consistently higher than the observed frequencies and are higher by roughly the quoted error of the observation. This is probably due to the heavy weighting of the 500 gauss results. Although these resonances are quoted with errors of 3 or 4 kilocycles per second corresponding to their full width at the base, it is conceivable that the possible effects of field instability and power shift have not been given sufficient weight. Thus, although the field calibration was the same before and after the run, there is no

definite assurance that the field had not shifted and returned to its initial value by the time the field was recalibrated. Since the amount of r.f. power being applied is not known, no definite numerical correction could be made for power shift, which, according to calculation, would amount to -2.5 kilocycles per second per 100 milligauss of r.f. field.

As pointed out in Chapter III, the effect of any power shift could be overcome by observing n' and n'' transition pairs for which the power shifts should be calculable. Only their frequency differences would be used to yield a direct measurement of μ_I (equation 3-28) while the lower field resonances, for which less power was necessary, would determine $\Delta\nu$. The data obtained at 340 gauss may be used to give a rough value for such a direct measurement of μ_I. Assuming again that n' transitions were observed, the $\nu(3'') - \nu(3')$ and $\nu(4'') - \nu(4')$ frequency difference give a value of $\mu_I = (4.29 \pm 0.07)$ nuclear magnetons. This value is in excellent agreement with that obtained from the computer fit, although its error is much larger than would prevail if the measurements at 500 gauss were possible.

5. The Silver-111m Experiment

An attempt was made to determine the nuclear spin of silver-111m ($T_{1/2}$ = 1.2 minutes) formed in the decay of palladium-111 ($T_{1/2}$ = 22 minutes). The latter isotope was produced by neutron bombardment of palladium-110 occurring in natural palladium. Palladium-110 has a natural abundance of 11.81% and has a thermal neutron capture cross-section of 0.36 barns.

A 100 milligram sample was irradiated for forty minutes in the pneumatic "rabbit" facility of the reactor. The sample was delivered directly to the radio-isotope laboratory adjoining the atomic beam labor-

atory . Source preparation and beam production was otherwise identical to that used in the silver-109m experiments.

Since natural palladium was used as source material, palladium-109 and, thus, silver-109m were also produced during the irradiation. At the end of irradiation, the ratio of silver-111m activity to silver-109m activity was calculated to be about one to three. The total beam intensity, that is, silver-109m activity plus silver-111m activity, was found to be a factor of about seventy lower than that obtained in the much longer irradiation used for the silver-109m experiment. It was impossible to perform the silver-111m experiment with such a small beam.

The silver-111m experiment was deferred until palladium enriched in palladium-110 becomes available. This enriched palladium is not available at present.

CHAPTER VI

THE CESIUM-138 EXPERIMENTS

1. Source and Beam Production

The cesium-138 ($T_{1/2}$ = 32 minutes) used in these experiments was produced from the decay of the fission-product xenon-138 ($T_{1/2}$ = 14 minutes). Since a detailed account of the procedure used for the extraction of the cesium is presented elsewhere (Archer, 1965), only a brief outline of the method will be given here.

The source consisted of 50 milligrams of UO_2^{++} ions (93% U^{235}) adsorbed on 5 grams of hydrated zirconium oxide ion-exchange crystals HZO-1 (available from Bio-Rad Laboratories, Richmond, California). An irradiation time of 5 minutes in a neutron flux of 10^{13} neutrons/cm^2/sec was used. The fission product gases were swept out and separated after 8 minutes of decay in the source. The xenon fraction was then swept into a constricted U-tube which was cooled in a liquid nitrogen bath and contained about 20 milligrams of CsCℓ crystals. Xenon-138, the major portion of the activity, was allowed to decay for 15 minutes, and the U-tube was then warmed and the remaining xenon swept out. This separation was done in the reactor by Dr. Archer, and the sealed U-tube containing one or two millicuries of active cesium was placed in a lead castle and brought to the radio-isotope laboratory adjoining the atomic beam apparatus.

All further source preparation took place in a fume-hood. Lead bricks provided shielding from the intense radiation (about 15 mr/hour at 1 foot through 1-1/2 inches of lead). The U-tube was broken below the

constriction, and the portion of the tube containing the CsCℓ crystals was washed down with a few drops of water which readily dissolved the crystals. The solution was then emptied into a small steel crucible and warmed to evaporate the water. After metallic sodium, to be used as reducing agent, had been added, the crucible was placed in the atomic beam oven which was then inserted into the machine. The oven was heated to an operating temperature of about 500°C. Between 15 and 20 minutes elapsed from the time of arrival of the source in the radio-isotope laboratory to the production of a beam.

A very intense sodium beam was produced first. This beam was used for oven alignment and also for field calibration throughout the experiment. The stable cesium beam was also used for a check on the field calibration. Typically, the entire source was evaporated from the oven in about twenty minutes.

Preliminary experiments with stable CsCℓ had been made using calcium, sodium, and lithium metals as reagents to produce a cesium beam. In order to evaporate 20 milligrams of source from the oven in twenty minutes, it was found that the oven had to be heated to about 600°C. when calcium metal was used. At this temperature, a CsCℓ molecular beam was produced, and much of the source was lost in this unusable form. When lithium and sodium metals were used, it was found that a much smaller molecular beam, and, hence, a larger atomic beam, were produced. Metallic sodium was used because it could be easily detected with the surface ionization detector and, thus, served also for both alignment and field calibration.

2. Beam Detection

Since the cesium atom has a large effective magnetic moment and is moving relatively slowly at the operating temperature used, most cesium

atoms undergo large deflections by the magnets. Consequently, few reach the detector even if the stop is removed (unless, of course, an appropriate radiofrequency is applied). The usual method of beam intensity measurement, that is, exposure of half-beam buttons, cannot be used in this case. Further, since the source was exhausted in twenty minutes, it was difficult to regulate the beam intensity by controlling oven heating. Because of the short half-life of the cesium, time could not be spent waiting for the beam to stabilize. Consequently, another type of beam intensity measurement was used - the double-collection technique.

This method of detection is based upon the following principles. In normal operation, the jaws of the B magnet exit slits are positioned about 0.010" or 0.015" on either side of the machine centre line. Any unfocussed or thrown-out portion of the beam which clears the B magnet pole-tips is then prevented from reaching the detector. In the double-collection technique, another stop is placed at the normal position of one exit slit jaw, and this slit jaw is then moved further away from the centre-line. This permits part of the thrown out beam to reach another appropriately placed detector. One edge of the stop and the other slit jaw define the usual exit aperture so that resonance exposures may still be made. At the same time, however, a monitor button may be exposed at the unfocussed beam position. Since the thrown-out beam is at all times proportional to the actual beam intensity, the ratio of the activity present on the resonance button to that present on the monitor button will automatically be normalized to any beam variations. These ratios may then be directly compared and a resonance will be evidenced by an increase in the ratio.

Figure 15 shows the variation of intensity with position behind the modified B magnet exit aperture. A beam of stable cesium was used.

FIGURE 15

The variation of beam intensity with position at the exit slit of the apparatus after installation of the double-collection stop. A stable cesium beam was used. The positions occupied by the monitor and resonance buttons are indicated.

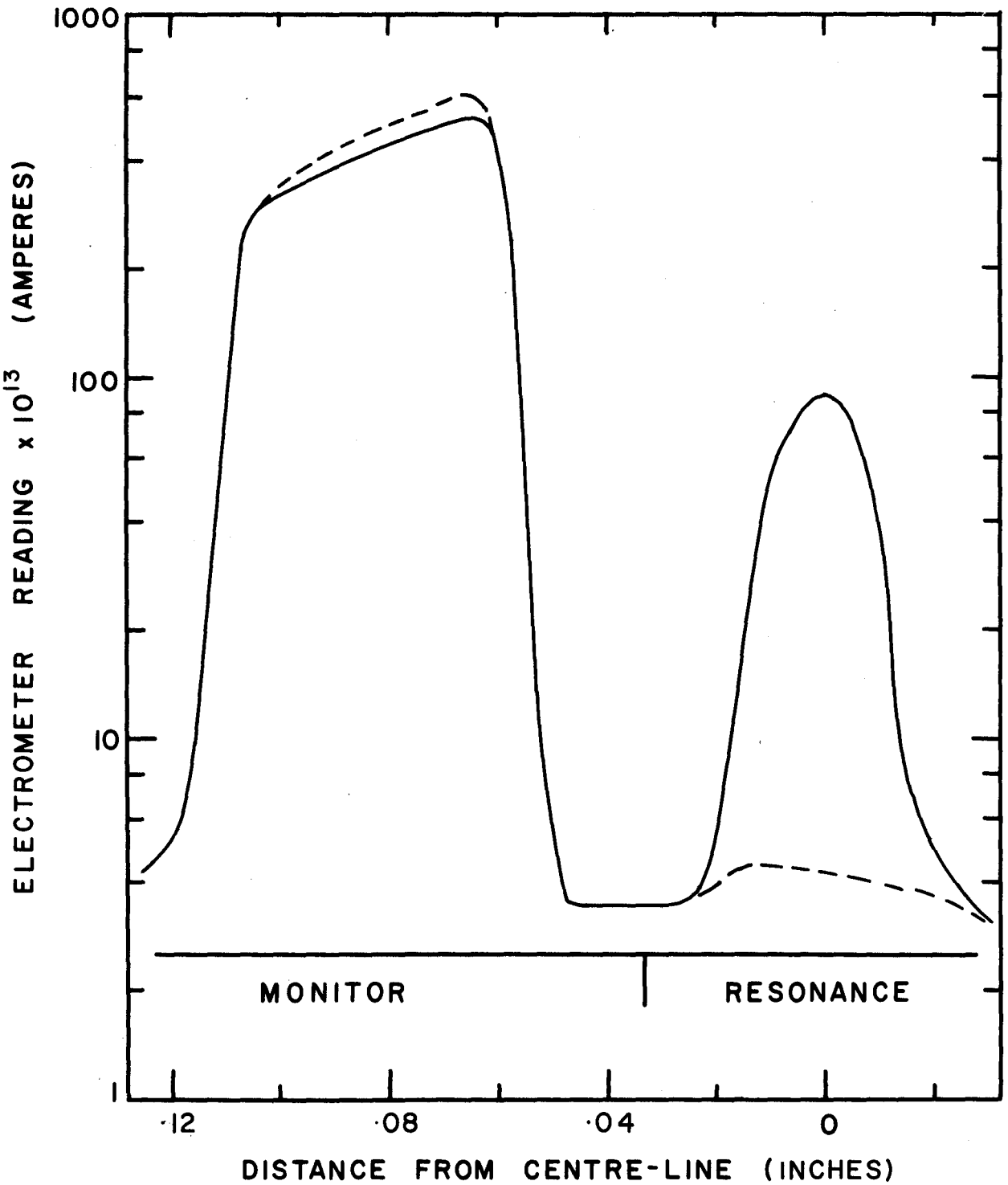
1000
100
10
1
ELECTROMETER READING x 10^13 (AMPERES)
MONITOR
RESONANCE
·12
·08
·04
0
DISTANCE FROM CENTRE-LINE (INCHES)

In this case, the slit jaw on the left hand side was moved. The solid line was obtained on resonance, and the dashed line was obtained with no r.f. applied. Monitor and resonance button positions are indicated.

3. Experimental Results

The C field was set to 5.6 gauss, and equation (3-17), using, of course, the g_J-value for cesium, was used to calculate the frequencies at which resonances should occur for integral spins from zero to seven. Exposures were made at these calculated frequencies. Since only four, and sometimes three, exposures could be made with each source, three sources were required for the spin search. Figure 16 shows the composite results for the three samples. Previous experiments, carried out with weaker sources and without the benefit of the double collection technique, had revealed that the spin was very likely three. Thus, a spin-3 exposure was made with each sample. The dashed line in Figure 16 is a visual average of the low points. Machine background was not determined experimentally.

It is apparent from Figure 16 that a spin-3 activity is present. Figure 17 shows the decays of a monitor exposure and a spin-3 exposure. The solid lines, drawn to correspond to a 32-minute half-life, are in excellent agreement.

Comparison of Figures 15 and 16, however, clearly shows that the off-resonance background was far from ideal. Several possible causes for this result can be suggested. The most obvious is that the monitor and resonance buttons were not properly placed. Had the resonance buttons been positioned such that some of the thrown out beam fell on them, the background would be significantly increased relative to that to be obtained on a properly placed button. Another possibility is that a large amount of

FIGURE 16

The results of the spin-search for cesium-138 at a field of 5.6 gauss. The dashed line is a visual average of the low points. No separate determination of machine background was made.

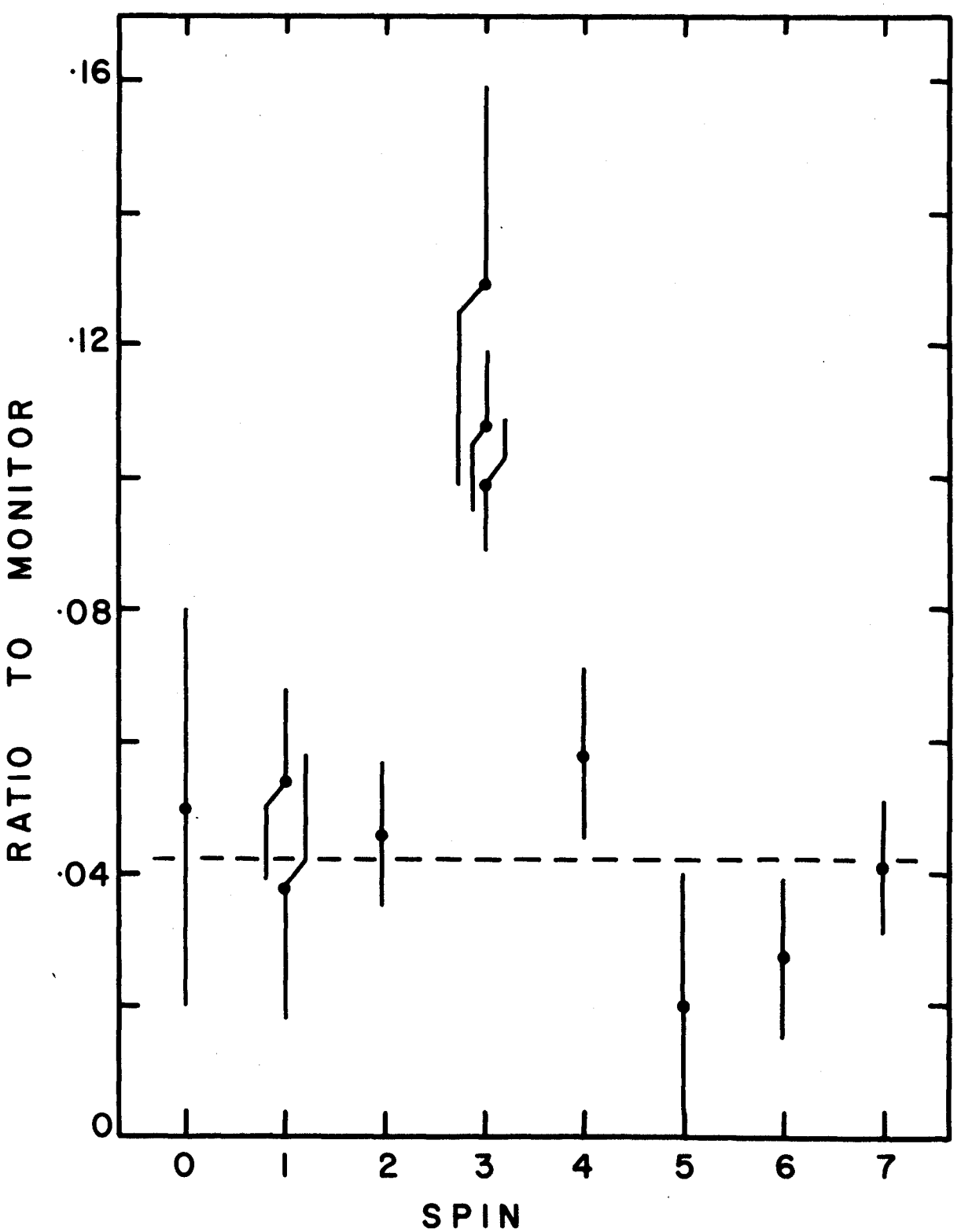
·16
·12
·08
·04
0
RATIO TO MONITOR
0
1
2
3
4
5
6
7
SPIN

FIGURE 17

Typical decay curves for the activity deposited on the buttons. The open and solid circles are for a monitor and resonance exposure respectively. The lines are drawn to correspond to a 32-minute half-life.

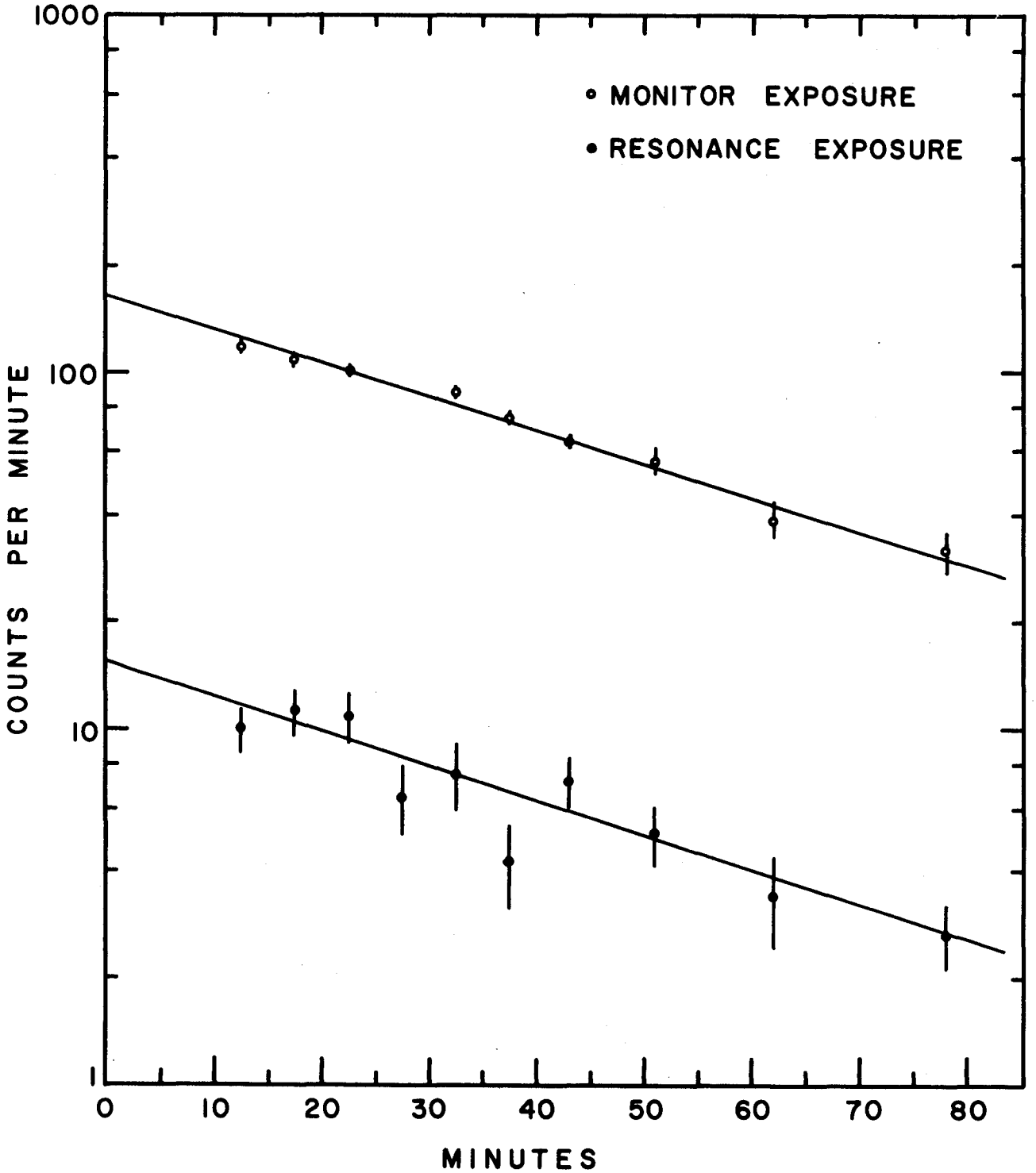
1000
100
10
1
COUNTS PER MINUTE
MONITOR EXPOSURE
RESONANCE EXPOSURE
0
10
20
30
40
50
60
70
80
MINUTES

gas scattering occurred, thus increasing the background on the resonance exposure. A third possibility is that the oven had not been properly aligned on the beam axis. Considering the beam profile shown in Figure 15 and the alignment of the oven with a sodium (and cesium) resonance, it is felt that the high background was caused mainly by gas scattering. This is not illogical since nearly twenty milligrams of cesium, together with a large amount of sodium, were evaporated from the oven in a short length of time.

Because of the radiation hazard in the source preparation, a total of five sources had been promised for the spin search. The remaining two sources were used in an attempt to obtain resonance shapes at higher fields. Figure 18 shows the results obtained at 12.40 and 24.05 gauss. The resonance at 12.40 gauss clearly shows a shift from the nominal frequency, that is, the frequency given by equation (3-17). Although only three exposures were obtained with the last sample at 24 gauss, a resonance shape similar to that obtained at 12 gauss is drawn through the points.

A significant shift in the resonant frequency at low field indicates a small hyperfine splitting. This can be seen from equation (3-25) with n=1 (none of the unusual transitions discussed in Chapter III will be focussable in the case of a small $\Delta\nu$). The shift observed at the lower and higher field can be used in conjunction with that equation to set an upper and lower limit, respectively, on $\Delta\nu$. Thus, the 12 gauss resonance peak is certainly no lower than 5.025 megacycles per second, and the 24 gauss "resonance" is certainly no higher than 10.025 megacycles per second. Ignoring the terms in μ_I in equations (3-24) and (3-25), it is found that

$$1400 < \Delta\nu < 2300 \qquad \text{Mc/sec.}$$

FIGURE 18

Resonance curves in cesium-138 obtained at 12.40 and 24.05 gauss. The arrow in the upper diagram indicates the expected frequency of a spin-3 resonance at 12.40 gauss. The curve in the lower figure was drawn, for illustrative purposes, similar in shape to the resonance obtained at 12.40 gauss.

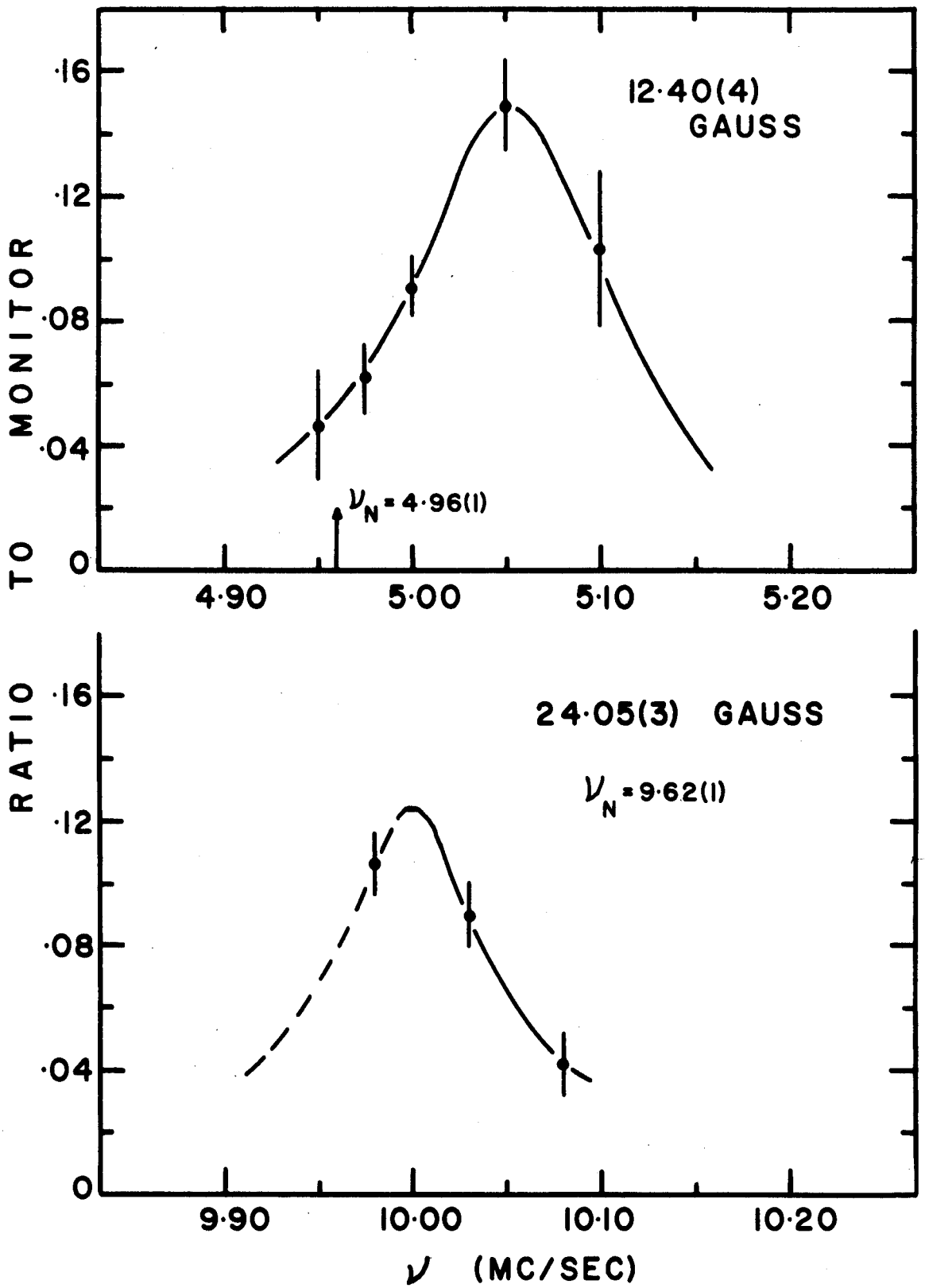
12·40(4)
GAUSS
ν_N = 4·96(1)
RATIO TO MONITOR
·16
·12
·08
·04
0
4·90
5·00
5·10
5·20
24·05(3) GAUSS
ν_N = 9·62(1)
9·90
10·00
10·10
10·20
ν (MC/SEC)

If the 12 gauss resonance is taken to occur at 5.050(25) megacycles per second, then that resonance alone gives a value

$$\Delta\nu = 1650 \begin{matrix}+650 \\ -350\end{matrix} \quad \text{Mc/sec.}$$

Thus, it seems safe to conclude from the two results that

$$\Delta\nu = 1650 \begin{matrix}+650 \\ -250\end{matrix} \quad \text{Mc/sec.}$$

At this point, these experiments were discontinued because of the health hazards in source production. When safer facilities become available it would be easy to follow the resonance to much higher fields and, hence, obtain an accurate value of $\Delta\nu$.

Using the Fermi-Segrè formula, equation (3-10), and (3-13), and the value for the hyperfine separation obtained above, the magnetic moment of Cs^{138} is found to be

$$|\mu_I| = 0.45 \begin{matrix}+0.18 \\ -0.07\end{matrix} \quad \text{nuclear magnetons}$$

uncorrected for diamagnetic shielding. The comparison isotope was taken as Cs^{133} ($I = 7/2$) for which $\Delta\nu = 9192.631770$ Mc/sec and $\mu_I = 2.5641$ nuclear magnetons. To the accuracy of the result, one need not give any consideration to the possibility of a hyperfine anomaly.

CHAPTER VII

DISCUSSION OF RESULTS

1. The Silver-109m Experiment

The spin search in silver-109m has established the spin to be $I = 7/2$. This result confirms the spin assignment inferred from conversion coefficient and half-life measurements (Nuclear Data Sheets, 1960).

Since the neighbouring even-even nuclei, palladium and cadmium, show vibrational states of the type expected in spherical nuclei, and since silver itself lacks only three protons from the closed proton shell at $Z = 50$, one would expect silver nuclei to be spherical. Thus, shell model considerations should be applicable, and the low-lying states should be explained in terms of the $g_{9/2}$ and $p_{1/2}$ proton levels which are in close competition just below the shell closure at $Z = 50$. This is borne out by the ground state spins as silver-105, -107, -109, -111, and -113 all have spin -1/2 and magnetic moments close to the Schmidt limit for a $p_{1/2}$ proton. In order to explain the observed spin of silver-109m, a proton configuration of $(g_{9/2})^{-3}_{7/2}$ must be assumed. The same assumption can be made to explain the ground state spin of silver-103 and the inferred spins of metastable states in silver-107, -111, and -113.

This particular type of coupling, that is, $(j)^{\pm 3}_{j-1}$, does not occur in the simple shell model, and, consequently, has been the subject of several investigations. In 1950, Kurath pointed out that such states could occur if the interaction between unpaired nucleons was assumed to have a finite range (Kurath, 1950). A study of the $g_{9/2}$-shell by Flowers failed

to produce any spin -7/2 states of lower energy than spin -9/2 states (Flowers, 1952). Talmi and Unna (1960) have considered nuclei at the beginning of the $g_{9/2}$ shell. Their results predict a low-lying spin -7/2 state if an appropriate effective nucleon interaction is used. Thankappan and co-workers have found a simple two-body potential which predicts spin -7/2 and spin -9/2 states of the same energy. The same potential, however, does not correctly predict energy levels in the $(p_{1/2})(g_{9/2})$ configuration (Thankappan et al, 1961). A pairing force calculation by Kisslinger and Sorensen (1963) does not produce a low-lying spin -7/2 state. It is pointed out, however, that had three quasi-particle states been included, important corrections would probably be introduced. In this case, the treatment would then be analogous to the calculations of Talmi.

It may be concluded from the above considerations that low-lying states of the type $(j)^{\pm 3}_{j-1}$ can arise if a shell model with interactions is employed. Since the position of these levels in the nuclear level scheme depends upon the residual interactions, a study of these anomalous coupling states will yield valuable information about nuclear forces.

As was explained in Chapter II (equation (2-5)), if a state of angular momentum I arises through the coupling of identical particles in a state j, then the magnetic moment of that state should be closely related to the magnetic moment of a single particle in the state j. In this instance, therefore, if silver-109m has the configuration $(g_{9/2})^{-3}_{7/2}$, it is to be expected that

$$\mu_{109m} = \frac{7/2}{9/2}\ \mu(g_{9/2}).$$

The Schmidt value for the moment of a $g_{9/2}$ proton is 6.79 nuclear magnetons. However, all of the known moments of nuclei of this type are quite a bit smaller. In particular, the moments of four indium nuclei, which have a

single hole in the $g_{9/2}$ level, are very closely the same, namely + 5.53 nuclear magnetons . Taking 7/9 of this value, one gets +4.30 nuclear magnetons in excellent agreement with the value for silver-109m measured in this work. This confirms beyond any doubt that the configuration of silver-109m is principally $(g_{9/2})^{-3}_{7/2}$. In fact, the agreement is so close that, whatever the mechanism is that causes the reduction of the moment from the Schmidt value, it is the same for silver-109m as for indium-109, -111, -113, and -115.

It is interesting to note that the magnetic moments of the odd-proton spin -9/2 nuclei between Z = 40 and Z = 50 are essentially constant after the third particle has been added to the $g_{9/2}$-shell. There is a slight decrease in moment as Z increases. Even more striking is the constancy with respect to the addition of neutron pairs as is seen in the sequence from indium-109 to indium-115. This is sharp distinction to the behaviour of the $p_{1/2}$ moments. In both silver and indium these show a steady trend, at the rate of about 0.02 nuclear magnetons per neutron pair, toward more negative moments.

These experiments have not been sufficiently accurate to definitely establish the existence of a hyperfine structure anomaly between silver-109 and silver-109m. The present data is fitted equally well if no anomaly is assumed. When a more stable field becomes available, it is intended to resume these experiments and, by observing corresponding n' and n'' transitions, make a precise determination of μ_I. The presence or absence of any hyperfine structure anomaly will then be established.

It is worth noting, however, that a hyperfine anomaly is to be expected. The distribution of nuclear magnetism due to the $p_{1/2}$ proton in

the ground state should be quite different than that for a $g_{9/2}$ proton. Recently, Easley and co-workers have made a calculation of the anomaly to be expected between Ag^{109} and Ag^{110m} (Easley et al, 1966). In that calculation, the effect of the odd-neutron in the latter isotope was ignored so that their result should also be, to a fair approximation, applicable to the case of $_{109}\Delta_{109m}$. There is the question, however, of the effect of the coupling that results in spin 7/2 rather than 9/2. When experimental conditions permit, it will be interesting to see what value the anomaly, if any, has.

2. The Silver-111m Experiment

This experiment showed that natural palladium cannot be used as source material for the study of silver-111m if the technique of the silver-109m experiment is used. A much larger source size than can be accomodated in the limited capacity of the high temperature oven would be necessary.

A source enriched to 90% in palladium-110 would provide about a four to one ratio in the activities of silver-111m to silver-109m. This would be a usable source for the silver-111m spin determination, but may be inadequate for further investigations of hyperfine structure. Since the specific activity of the enriched palladium-110 sources will be lower than that of the sources used in the silver-109m experiment, the oven might still have to be modified to contain a larger sample. At least it has been verified in the silver-109m experiments that essentially all the palladium remains in the oven. Thus, it should be possible to use the material over and over, keeping the cost of the source within reasonable bounds.

3. The Cesium-138 Experiment

In these experiments, it was determined that cesium-138 has I=3. This value agrees with the spin assignment inferred from decay scheme studies by Archer (Archer, 1965).

The shell model predicts that the 55^{th} proton and the 83^{rd} neutron should be in $g_{7/2}$ and $f_{7/2}$ levels respectively. Indeed, these states are found as the ground states in many neighbouring odd-Z and odd-N nuclei, for example $_{55}Cs_{82}^{137}$ and $_{58}Ce_{83}^{141}$. According to the coupling rules of Nordheim or Brennan and Bernstein, cesium-138 should then have a ground state spin of six, in disagreement with the experimental value. Also, in $_{57}La_{83}^{140}$, the measured spin is 3 while the prediction is 6. So there is a precedent for the failure of the semi-empirical rules in this region. On the other hand, for both $_{55}Cs_{79}^{134}$ and $_{57}La_{81}^{138}$, for example, the predictions are borne out.

One can also use the observed magnetic moment to provide a rough check on the odd particle assignments via equation (2-4). Taking the magnetic moment of the $g_{7/2}$ proton as + 2.80 nuclear magnetons (as approximately found in $Cs^{135,137}$ and La^{139}) and that of the $f_{7/2}$ neutron as -0.97 (as in Ce^{141}), the expectation for a spin-3 cesium-138 would be μ_I = +0.78 nuclear magnetons. The agreement with the experimental value, $0.45^{+0.18}_{-0.07}$ nuclear magnetons with the sign undetermined, is not good. This seems to indicate either that the odd particles are not in the levels indicated or that the interaction that results in spin 3 rather than 6 also causes a considerable alteration in the magnetic moment.

Further work with cesium-138 is anticipated as soon as safe facilities for source production become available. It is hoped that a more precise determination of the magnetic moment will allow interpretation of

the nucleon configuration in cesium-138.

4. Experimental Technique

In the course of this work, several experimental techniques new to this laboratory were utilized. Furthermore, the observation and analysis of transitions of a type not previously focussed in a flop-in atomic beam apparatus has been carried out.

The beam used in the silver experiments was produced by diffusing carrier-free radioactive silver out of palladium metal. This technique is possible, of course, only when the vapour pressure of the parent element is less than that of the daughter. It has the advantage that no chemistry is necessary in order to separate the daughter activity. More important, it means that the supply of the daughter material in the oven is continuously regenerated as the parent nuclei decay. This diffusing technique made possible the silver-109m experiment. Thus, in spite of the 41-second half-life of the silver, the 13.5-hour half-life of the palladium-109 parent ensured that a silver beam could be produced for as long as desired. The same technique could be used, for example, to study rhodium isotopes produced from radioactive ruthenium.

The silver-109m experiments have also shown a new technique for the direct determination of the nuclear magnetic moment. This method, which is particularly useful for isotopes with large hyperfine separations, requires the observation of corresponding transitions in both the $F = I + 1/2$ and $F = I - 1/2$ multiplets. Since these transitions are Zeeman transitions, special r.f. equipment is not required as is usually the case when direct hyperfine transitions are observed. A disadvantage of this new method is that very good stability is required at sufficiently high fields that the difference in frequency between the n' and n'' transitions can be determined

with the desired accuracy. Unfortunately, the lack of it in these experiments made a precise determination of the nuclear moment of silver-109m impossible. From the 340 gauss observations, however, a value of $\mu_I = 4.29 \pm 0.07$ nuclear magnetons was obtained.

The cesium-138 experiment was the first experiment done in this laboratory using the double collection technique. The results were quite promising, and this technique will undoubtedly be used in the future in experiments with low activities or short half-lives.

The cesium-138 experiment has also shown that atomic beam techniques can be used to determine the nuclear properties of short-lived fission products. Although such sources have low activity by atomic beam standards, it has been shown that modifications of technique will permit measurements to be made.

BIBLIOGRAPHY

Archer, N.P. 1965. Ph.D. Thesis, McMaster University.

Arima, A. and Horie, H. 1954. Progr. Theoret. Phys. (Japan) 11, 509.

Bardeen, J., Cooper, L.N. and Schrieffer, R. 1957. Phys. Rev. 108,1175.

Bellamy, E.H. and Smith, K.F. 1953. Phil. Mag. 44, 33.

Belyaev, S.T. 1959. K. Danske Vidensk. Selsk. mat.-fys. Medd. **31** No. 11.

Blin-Stoyle, R.J., and Perks, M.A. 1954. Proc. Phys. Soc. A67, 885.

Bohr, A. 1951a. Phys. Rev. 81, 134.

Bohr, A. 1951b. Phys. Rev. 81, 331.

Bohr, A. 1952. K. Danske Vidensk. Selsk. mat.-fys. Medd. 26, No. 14

Bohr, A. and Mottleson, B. 1953. K. Danske Vidensk. Selsk. mat.-fys. Medd. 27, No. 16 .

Bohr, A. and Weisskopf, V.F. 1950. Phys. Rev. 77, 94.

Breit, G. and Rabi, I. I. 1931. Phys. Rev. 38, 2082.

Brennan, M.H. and Bernstein, A.M. 1960. Phys. Rev. 120, 927.

Cameron, J.A. 1962. Ph.D. Thesis, McMaster University.

Cameron, J.A., King, H.J., Eastwood, H.K. and Summers-Gill, R.G. 1962. Can. J. Phys. 40, 931.

Davydov, A.S. and Filippov, G.F. 1958. Nuclear Phys. 8, 237.

Easley, W., Edelstein, N., Klein, M.P., Shirley, D.A. and Wickman, H.H. 1966. Phys. Rev. 141, 1132.

Eastwood, H.K. 1964. Ph.D. Thesis, McMaster University.

Eisinger, J. and Jaccarino, V. 1958. Revs. Mod. Phys. 30, 528.

Elliott, J.P. and Lane, A.M. 1957. Encyclopedia of Physics, ed. S. Flügge, Vol. XXXIX, 241. (Berlin: Springer -Verlag).

Fermi, E. 1930. Z. Phys. 60, 320.

Flowers, B.H. 1952. Proc. Roy. Soc. A 215, 398.

Freed, N. and Kisslinger, L.S. 1961. Nuclear Phys. 25, 611.

Gerlach, W. and Stern, O. 1921. Z. Phys. 7, 249.

Hack, M.N. 1956. Phys. Rev. 104, 84.

Haxel, O., Jensen, J.H.D. and Suess, H.E. 1948. Naturwiss. 35, 375.

Honig, R.E. 1962. R.C.A. Review, December, 527.

King, H.J. 1960. Ph.D. Thesis, McMaster University

Kisslinger, L.S. and Sorensen, R.A. 1960. K. Danske Vidensk. Selsk. mat.-fys. Medd. 32, No. 9.

Kisslinger, L.S. and Sorensen, R.A. 1963. Revs. Mod. Phys. 35, 853.

Kopfermann, H. 1958. Nuclear Moments (trans. E.E. Schneider, Academic Press, New York).

Kurath, D. 1950. Phys. Rev. 80, 98.

Mayer, M.G. 1948. Phys. Rev. 74, 235.

Mayer, M.G. 1950. Phys. Rev. 78, 16.

Nilsson, S.G. 1955. K. Danske Vidensk. Selsk. mat.-fys. Medd. 29, No.16.

Nordheim, L.W. 1951. Revs. Mod. Phys. 23, 322.

Nuclear Data Sheets 1960. Nuclear Data Sheet 60-2-54, Nat. Academy of Sci. N.R.C. (U.S.A.)(U.S. Gov't. Printing Office).

Rabi, I.I. 1937. Phys. Rev. 51, 652.

Rabi, I.I. , Zacharias, J.R., Millman, S. and Kusch, P. 1938. Phys. Rev. 53, 318.

Ramsey, N.F. 1956. Molecular Beams (Oxford University Press).

Salwen, H. 1956. Phys. Rev. 101, 623.

Schmidt, T. 1937. Z. Phys. 106, 358.

Schwartz, C. 1955. Phys. Rev. 97, 380.

Stroke, H.H. 1959. Quarterly Progress Report No. 54. Research Laboratory of Electronics, M.I.T., July 15.

Stroke, H. H. and Blin-Stoyle, R.J. 1961. Phys. Rev. 123, 1326.

Talmi, I. and Unna, I. 1960. Nuclear Phys. 19, 225.

Thankappan, V.K., Waghmere, Y.R. and Pandya, S.P. 1961. Progr. Theoret. Phys. (Japan) 26, 22.